RNA Targets and Function of *Topoisomerase 3β* in Reducing Cellular Stress

Shohreh Teimuri and Beat Suter*

Institute of Cell Biology, University of Bern, Berne, 3012, Switzerland

*Corresponding address: Beat.Suter@unibe.ch

Keywords: Topoisomerase 3β, Drosophila, RNA topoisomerase targets, posttranscriptional gene expression, cellular stress, neurodegeneration, cancer.

Abstract (217 words)

Topoisomerase 3β (Top3β) relaxes DNA and RNA, and it is the only Topoisomerase found to work on RNAs. We isolated and identified the naturally cross-linked RNA targets of Top3β in Drosophila. Top3β is particularly active on long RNAs, RNAs with many splice sites, and RNAs that are localized in large cells. Demonstrating the importance of its enzymatic activity, Top3β without the hydroxyl group that is needed for its covalent binding to the RNA, prevents normal expression and subcellular localization of the gene products of the identified targets. At the cellular level, Top3β activity is needed to maintain the morphology of the neuromuscular junction in adult flies and to prevent premature loss of coordinated movement and aging. Alterations in human *Top3β* have been associated with several neurological diseases and cancers. The homologs of genes and (pre)mRNAs mis-expressed in these conditions show the same characteristics identified in the Drosophila *Top3β* targets, suggesting that the Drosophila can model the function of human *Top3β*. Testing the role of the enzymatic activity of Top3β in the ALS/FTD-associated RNA $(G4C2)_{49}$ assay for neurodegeneration, revealed that *Top3β*$^{+}$ clearly reduced the neurodegenerative activity of this RNA. Therefore, this study not only identified RNA targets of Top3β but also showed the physiological relevance of the enzymatic activity of Top3β toward its RNA targets in different situations.

Introduction

Topoisomerase 3β (Top3β) is an RNA-binding protein (RBP) with dual enzymatic activity toward DNA and RNA (1). Topoisomerases are better known for their activity toward DNA, where they resolve tension and supercoiling. Much less is known about the function of topoisomerases toward RNA. Along with other RBPs, Top3β contributes to mRNA translation, particularly in the nervous system, which is significant for neurodevelopment and psychological and physical well-being (2). Its functional importance is suggested by results that link impaired *Top3β* function to various neurodevelopmental and cognitive disorders (2)(3)(73).

Drosophila melanogaster Top3β possesses the key features of a topoisomerase. The predicted catalytic tyrosine (Tyr, Y) residue is present at position 332 (Y332) and is essential for its topoisomerase activity (4). Top3β topoisomerases distinguish themselves from other topoisomerases by their conserved RNA-binding motif called RGG (Arginine Glycine Glycine) box, which binds to RNAs or proteins. Its paralogue Top3α, a DNA topoisomerase, possesses the catalytic tyrosine residue but lacks the RGG box (4). *In vitro*, the RGG box is not required for the enzymatic activity but might play a role in binding to the RNA and thereby facilitating the enzymatic activity *in vivo* (2).

We hypothesized that the neurological requirements for an RNA topoisomerase might reflect, in part, its activity on mRNAs that need to be transported over long distances to be translated at the right place and at the right time. During such transport, long molecules, such as mRNAs, are likely to become entangled or suffer other structural problems that might interfere with their packaging, transport, unpackaging, and translation (1). A topoisomerase that acts on RNAs might, therefore, be able to rescue such RNAs. As discussed by Su and colleagues (74), there is considerable evidence that Top3β activity on RNA has important functions in cells and that it might act at all levels of gene expression. Using human cell lines, these authors showed that Top3β indeed affects mRNA translation and turnover (74). However, there is still surprisingly little knowledge about the steps in gene expression where Top3β acts on RNAs and particularly about the *in vivo* role of this activity for the cells and the organism. Especially in large cells, where mRNAs need to travel over long distances, an RNA topoisomerase could provide an important advantage and allow the cell to function properly. Drosophila has such

large cells in the nervous system, the female germline, and the young, syncytial embryo. The latter is easily accessible and free of additional tissue. The expression of Drosophila Top3β is particularly abundant in 0-2 hours old, syncytial embryos. In these large cells, proper mRNA localization to specific compartments combined with controlled local translation is essential for normal differentiation and cellular physiology. We, therefore, set out to study the activity and function of Drosophila Top3β in young embryos to identify relevant *in vivo* RNA targets, interacting proteins, and biological functions.

Consistent with the notion that larger RNAs are more likely to encounter structural problems in living cells, we found that longer RNAs are more likely to be targets of Top3β in young embryos. This seems significant because the same RNA features are also over-represented among the differentially expressed RNAs in the *Top3β* mutants. Specific mutations of the Y332 active site tyrosine (Y332F) and the RGG box (ΔRGG) revealed the importance of the enzymatic activity and the RNA/protein binding, respectively. The enzymatic activity of Top3β is needed to bind to mRNAs and for the normal accumulation of these mRNAs and their encoded proteins in general and in specific subcellular locations. The lack of this enzymatic activity stresses the affected cells and causes neurodegeneration and premature aging. Because human Top3β affects the expression of RNAs with similar features and the Drosophila enzyme affects the outcome of a human RNA that causes neurodegeneration, this Drosophila model produces valuable novel insights into neurodegenerative diseases and cancers with which human *Top3β* had been associated.

Results

RNAs depending on *Top3β* for their normal expression

To test whether Top3β affects RNA expression, RNAs from 0-2 hours-old embryos were extracted from a wild-type control strain and the *Top3β* mutants *Top3β*^{26}, *Top3β*^{Y332F}, and *Top3β*$^{\Delta RGG}$. All mutants were both maternally and zygotically mutant. Sequence analysis of the transcriptome carried out on biological triplicates established the effect of the different *Top3 β* mutations on the RNA levels expressed in 0-2 hours old embryos. Transcriptome-wide changes in RNA levels between the *Top3β* null mutant *Top3β*^{26} and the wild type were analyzed and RNAs that showed level changes in adjusted p-values <0.05 and absolute log2 fold changes >1 were selected for further analysis (**Supplementary Tables S1, Fig. 1**). This yielded 677 differentially expressed RNAs of which 73% (496) were downregulated in the null mutant *Top3*^{26}. The effect of *Top3β* on the different RNA levels can either be direct or indirect. Under the assumption that direct effects on RNAs help to rescue RNAs and indirect effects could evenly cause up or downregulation of RNA levels, the estimated number of RNAs directly dependent on *Top3β* for their normal expression levels would be around 315.

Gene ontology enrichment analysis on the list of genes that depend on *Top3β* for their normal expression revealed an enrichment for biological processes associated with different aspects of cellular development and physiology (**Supplementary Fig. S1**). Several of these are active in neural processes, including the regulation of axon extension and guidance, and the regulation of synaptic vesicles. This points to the possible effects of Top3β on neuronal processes. We also noted the enrichment of several other processes relating to cellular signaling, regulation of the cytoskeleton, and meta-/catabolic processes.

To investigate the contribution of the catalytic Tyr (which is essential for the enzymatic activity) and the RGG domains (which mediates interactions with RNAs and proteins) to the proper expression of these 677 differentially expressed genes, their expression was also analyzed in both point mutants (**Fig. 1A**). In the *Top3β*^{Y332F} mutant, 220 out of 289 (76%) differentially expressed RNAs were downregulated in the embryos. This fraction is very close to the one of the null mutant, suggesting again, that the majority of these RNAs depend directly on the catalytic activity of Top3β. The impact of the mutated RGG domain on the embryonic transcriptome was less pronounced, with 29 out of 61 (47%) RNAs downregulated

110 in the embryo, many might be indirect targets. Remarkably, 2 out of 3 of these RNAs
111 depended not only on the RGG motives but also on the Y332 for their normal expression
112 levels.

113 To focus more on the direct consequences of *Top3β* activity, we selected the embryonic RNAs
114 that depended on *Top3β* for their normal level of expression and were downregulated in the
115 null mutant **(Supplementary Table S1).** We then asked which RNA features were
116 overrepresented in this group compared to the wild-type control. In embryos, the RNAs that
117 were downregulated in the *Top3β*^{Y332F} and *Top3β*^{26} mutants had longer untranslated regions
118 (UTRs), protein coding sequences (CDS), and pre-mRNAs (**Fig. 1B-1D**). We conclude that long
119 pre-mRNAs and mRNAs depend more strongly on *Top3β* to reach their normal expression
120 levels.

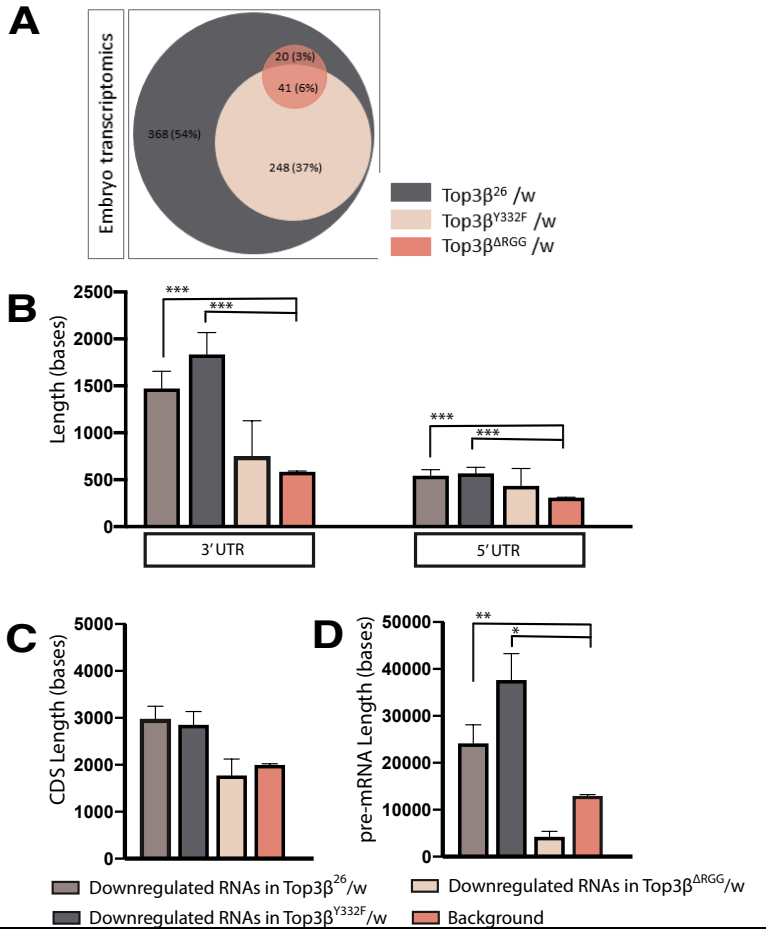

121

122 **Fig. 1. Effect of the *Top3β* mutations on the embryonic transcriptome. A)** Effect of the *Top3β* point
123 mutations on the expression of the 677 genes that are differentially expressed in the *Top3β* null mutant
124 *Top3β*^{26}. The number and percentage of differentially expressed RNAs in 0-2 hrs. old embryos are
125 shown. Expression levels were determined relative to the transcript levels of the *Top3β*$^{+}$ strain *w*. **B)-D)**

126 RNA features of transcripts that depend on *Top3β* to reach normal expression levels. **B)** mRNAs with
127 longer UTRs are over-represented in the group of RNAs that depend on *Top3β* to reach normal
128 expression levels. **C)** mRNAs with longer CDS are more downregulated in the $Top3\beta^{26}$ and $Top3\beta^{Y332F}$
129 mutants. **D)** mRNAs with longer pre-mRNAs are more downregulated in the $Top3\beta^{26}$ and $Top3\beta^{Y332F}$.
130 Expression levels were compared to the $Top3\beta^{+}$ (*w*) control in 0-2 hrs. old embryos. p-value
131 <0.0001=****, p-value <0.001=***, p-value <0.01=**, p-value <0.05=*

132

133 ***Top3β* in neurological diseases and cancers**

134 *Top3β* has been associated with several neurological diseases and cancers. To test whether
135 the human *Top3β* acts also to support the expression of higher levels, particularly of long
136 RNAs, a list of diseases associated with *Top3β* was retrieved using gene-disease associations
137 (DisGeNET (v7.0)(5)). This list consisted of 12 diseases which were either neurological diseases
138 or cancers. The lists of differentially expressed genes associated with each of these diseases
139 were then obtained from the same database and used to identify their *Drosophila*
140 orthologues from DIOPT Version 9.0 (**Supplementary Table S2**). The list of these *Drosophila*
141 genes was then compared with the list of genes whose embryonic mRNAs are downregulated
142 in the absence of *Top3β* (**Supplementary Table S1**) to identify the genes shared between the
143 two lists (**Fig. 2**). Due to the very short list of shared genes with the Juvenile Myoclonic
144 Epilepsy (JME), this disease was not considered for further studies. For the remaining ones,
145 there is a clear overlap between the two datasets and the overlap ranges between 2 and >3
146 times the calculated random overlap, suggesting that the effects seen in the fly model with
147 the inactivated *Top3β* also contribute to the human disease phenotype.

148 Notably, a single gene, *Rop* (*Ras opposite*), was present in the lists from all neurological
149 diseases and the downregulated embryonic RNAs (**Fig. 2C**). *Rop,* is involved in vesicle release
150 and control of synaptic activity (6)(7). In contrast, comparing all cancer lists with the
151 downregulated embryonic RNAs in the *Top3β* mutants, revealed 50 genes shared between
152 the six different lists (**Figs. 2D, E**). Based on the KEGG pathways, some of these shared genes
153 are only involved in the MAPK (mitogen-activated protein kinase) signaling pathway that
154 regulates various cellular processes, including cell growth, proliferation, differentiation, and
155 survival (8) (9). It thus seems that the MAPK signaling pathway is particularly sensitive to
156 *Top3β* activity and that this might affect growth control.

157

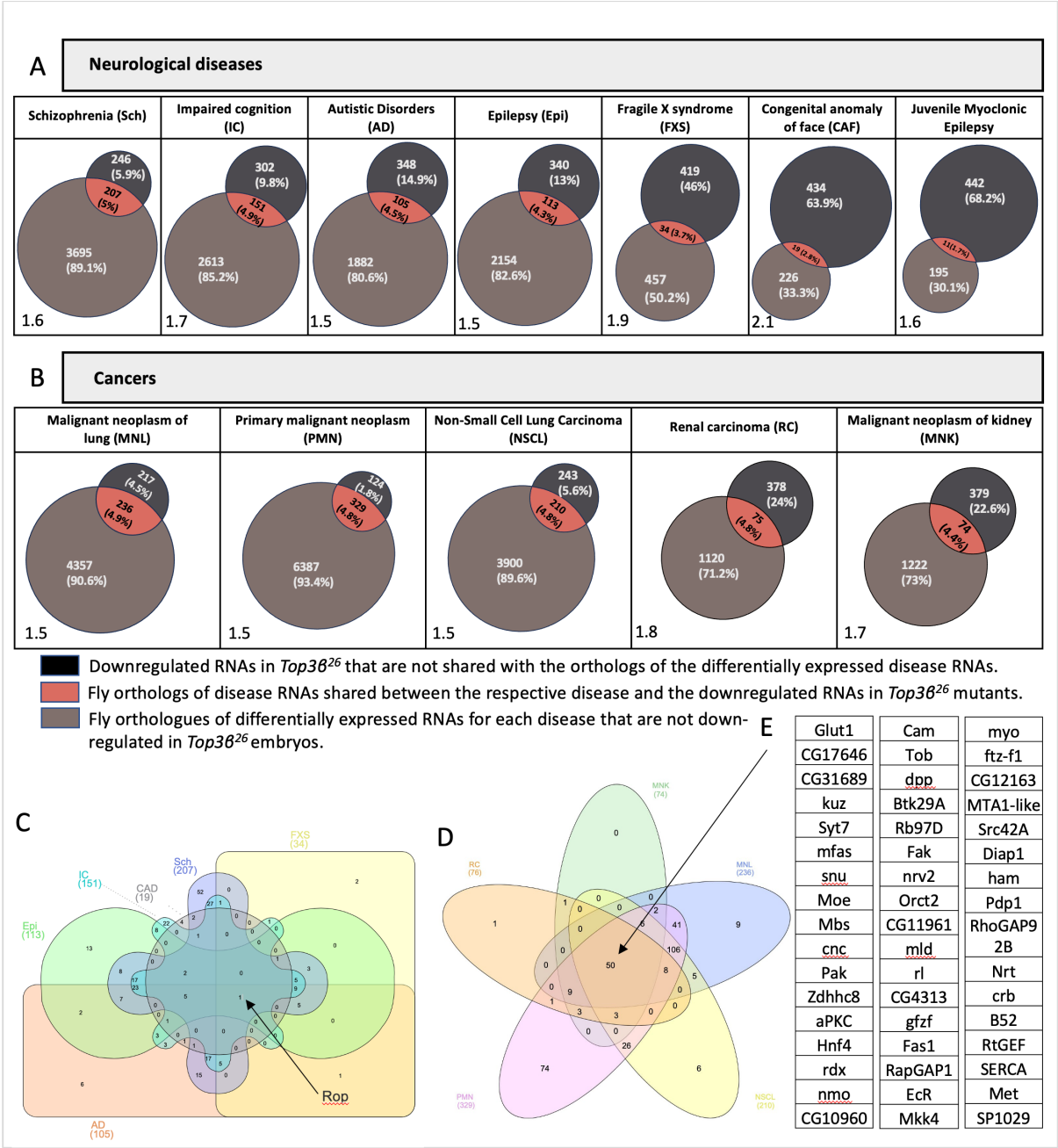

Fig. 2. Overlap between downregulated embryonic RNAs in *Top3β*^{26} and the fly homologs of differentially expressed RNAs in cancers and neurological diseases. A, B) Venn diagram of the genes shared between the list of down-regulated RNAs in *Top3β*^{26} embryos and the fly homologs of differentially expressed RNAs of the listed diseases. Numbers and frequencies are listed. The probability of random overlap is shown in % at the bottom left of each Venn diagram. **C)** Drosophila genes depending on *Top3β* for normal expression levels in embryos were placed into a Venn diagram such that their position shows in which neurological disease their homologs also depend on (human) *Top3β* for their normal expression levels (note that JME was not included). *Rop* appeared in all lists. **D)** Drosophila genes depending on *Top3β* for normal expression levels in embryos were placed into a Venn diagram such that their position shows in which cancer their homologs also depend on (human) *Top3β* for their normal expression levels. **E)** List of the 50 genes that depend on *Drosophila Top3β* for their normal expression levels in embryos and whose homologs are also affected in all listed cancers associated with human *Top3β* alterations.

172

173 Comparing the features of the Drosophila RNAs shared between the fly list of embryonic RNAs
174 that depend on *Top3β*, and the homologs of the above human disease datasets revealed that
175 the RNAs shared between the two datasets had on average longer pre-mRNAs and UTRs
176 compared to the RNAs of the individual diseases that were not present in the embryonic list
177 **(Supplementary Fig. S2**). This result suggests that human *Top3β* also affects the expression
178 of RNAs with the same features as its fly homolog, pointing to the potential value of
179 identifying direct Top3β target mRNAs in the model system because their lower expression
180 might contribute to the disease phenotype.

181

182 **RNA interactions of Top3β**

183 To identify directly the RNA targets to which Top3β binds and performs its topoisomerase
184 activity, we sequenced the RNAs attached to Top3β::eGFP by immunoprecipitation (IP) in the
185 presence of (limited amounts of) ionic detergent. This was done using animals that expressed
186 an eGFP fused to wild-type Top3β and, as a negative control, Top3β::eGFP in which Y332 was
187 replaced by a phenylalanine (Y332F). This mutant form of Top3β lacks only the -OH group
188 through which Top3β forms the transient covalent bond between its Y332 side chain and the
189 RNA target during the enzymatic reaction (10). The naturally occurring covalent bond
190 between Top3β and its targets makes artificial cross-linking superfluous (thus reducing the
191 problem of high background) while still allowing the use of ionic detergents at low
192 concentrations during the isolation. These conditions should pull down primarily covalently
193 bound RNAs without denaturing the antibodies and their interactions. The covalent bond
194 between Top3β's Y332 and the RNA targets was stabilized for the IP by removing Mg^{2+}, which
195 is needed for the enzyme to resolve the bond at the end of the enzymatic reaction (11). To
196 determine if the target RNAs were specifically bound to the –OH group of Y332, we used the
197 Y332F mutant as a negative control as described above. The RNAs that are enriched in the
198 wild type compared to the Y332F mutant are candidate targets of the catalytic activity of
199 Top3β **(Supplementary Table S3)**. Because long RNAs seem more likely to depend on this
200 enzymatic activity, we further tested the quality of the data by comparing the RNA length of
201 the presumed targets with the background RNA length and found that longer RNAs were

202 more likely to covalently bind to Top3β as they showed higher enrichment in the wild-type
203 embryonic extracts (**Fig. 3A**). The results might also reflect that longer RNAs have a higher
204 chance of enduring physical stress and are also, for this reason, more likely to become
205 substrates of the enzymatic activity of Top3β. Interestingly, recent work in human cells also
206 found that TOP3β preferentially binds to long mRNAs (74).

207 From the list of immunopurified RNAs, the ones with an adjusted p-value smaller than 0.05
208 (adjp-value<0.05; note that *Rop* had 0.027) and a log2-fold change of more than 1 (log2FC>1)
209 were selected and ranked based on their adjp-value. These 46 embryonic RNAs and their
210 genes were used for further analyses (**Supplementary Table S4**). Several features of their RNA
211 correlated with the chance of becoming a target of Top3β's enzymatic activity. Top3β RNA
212 targets had on average longer 3'UTRs and stemmed from larger genes with longer introns
213 compared to the complete set of different types of RNAs detected in the wild-type RNA-IP
214 (**Fig. 3B-C, Supplementary Tables S3, S4)**. The fact that targeted mRNAs have longer 3'UTRs
215 is consistent with mRNAs that undergo localization and/or translational regulation having a
216 higher chance of becoming a Top3β target because these processes are mainly controlled by
217 sequences in the 3'UTR. A higher abundance of mRNAs with long coding sequences (CDS)
218 might reflect that mRNAs with long open reading frames (ORFs) might become a Top3β target
219 when their translation becomes blocked. Embryonic Top3β targets had also a higher number
220 of transcript isoforms per gene and more exons (**Fig. 3D-E, Supplementary Tables S3, S4)**.
221 This might indicate that mRNA splicing, a nuclear activity, increases the chance of an RNA
222 becoming a Top3β target. In summary, these results present evidence for the involvement of
223 Top3β in mRNA splicing, mRNA localization, and/or translational control and translation.

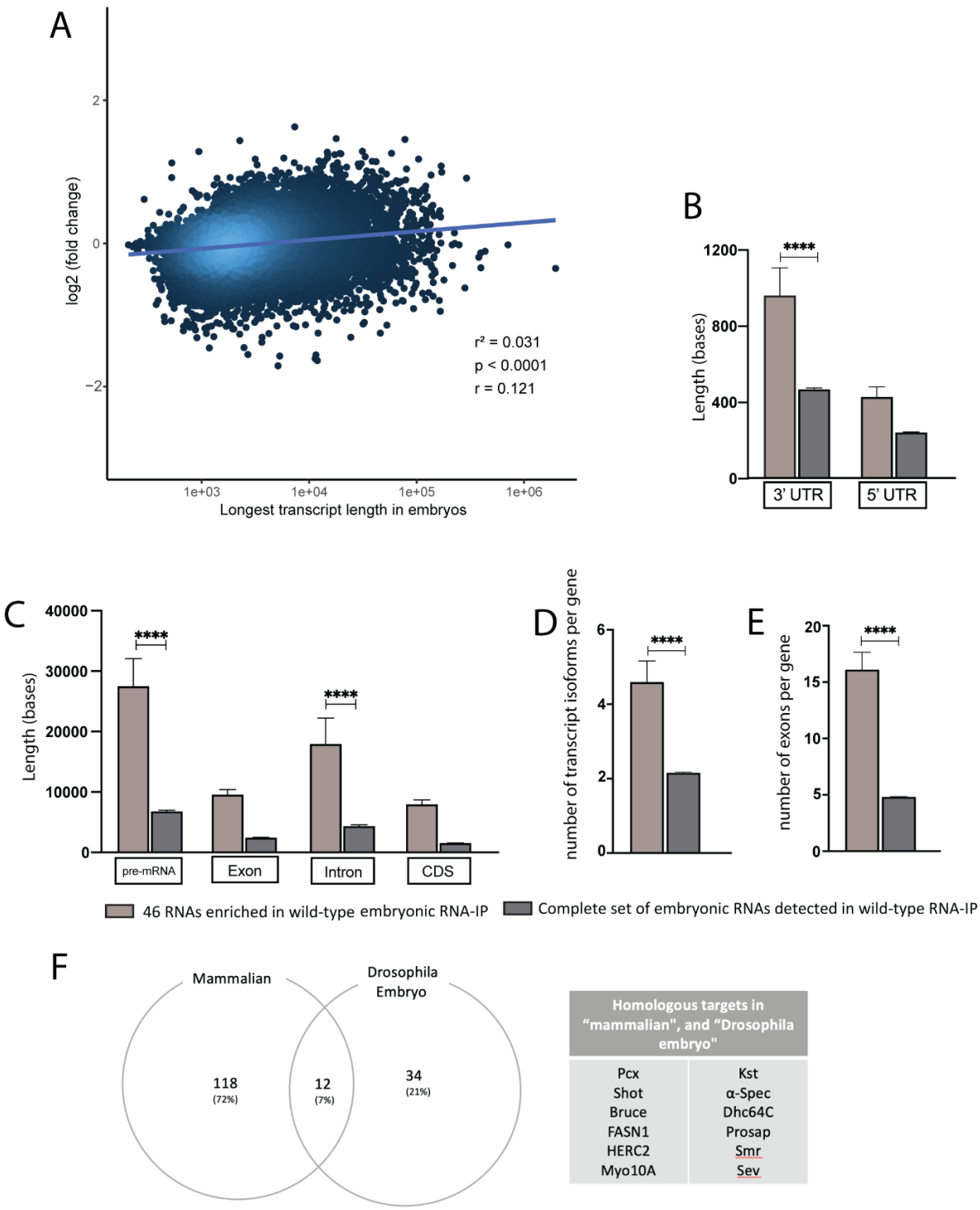

Fig 3: Characteristics of embryonic RNA targets of Top3β. A) Longer RNAs are more likely targets of the enzymatic activity of Top3β because they are more enriched in the IP with the wild-type Top3β compared to the Top3β^{Y332F}. r measures the strength of the correlation and p stands for p-value. **B-E)** Transcript features of the top 46 embryonic RNA targets of Top3β. The complete sets of RNAs detected in the wild-type RNA-IP served as the standard. p-value <0.0001=****, p-value <0.001=***, p-value <0.01=**, p-value <0.05=*. **F)** Homologous targets shared between Drosophila Top3β and mammalian FMRP1 and Top3β. Venn diagram for the RNAs shared between our study with the previous mammalian study (1), which revealed the overlap of the interactors with mouse FMRP1 from brain extracts and Top3β interactors in HeLa cells. The list of the Drosophila homologs that were also found in both mammalian interactor screens is also shown.

235 **Homologs of Drosophila Top3β target mRNAs also bind mammalian Top3β and FMR1**

236 The analysis of protein interactors of Drosophila Top3β showed that one branch of
237 interactions goes through Tdrd3 and FMR1, the fly homolog of FMRP (**Supplementary Fig.**
238 **S3**). Mammalian Top3β has been linked to the fragile X syndrome protein FMRP (1) which
239 binds to ribosomes and regulates translation. These researchers also found an overlap in HITS-
240 CLIP data of FMRP produced from mouse brain extracts and Top3β HITS-CLIP data of Flag-
241 Top3β from HeLa cells. Comparing the Drosophila Top3β::eGFP RNA-IP results with the shared
242 mammalian result set revealed intriguing similarities despite comparing different species and
243 having used different tissues (**Fig. 3F**). This further strengthens the value of the technique
244 applied to obtain the Drosophila Top3β target RNAs and the use of Drosophila as a model to
245 study the role of Top3β in human disease. A Venn diagram illustrates the overlap between
246 the top targets of Drosophila Top3β and the shared mammalian targets, with the number of
247 such overlapping targets listed (**Fig. 3F**). The common feature of the proteins encoded by the
248 shared RNA targets is that they are predominantly large proteins. Many are localized to the
249 plasma membrane or the cell cortex (e.g., Sev, Mgl, α-Spec, Kst, Pcx) or cytoskeleton-
250 associated (e.g., Dhc64C, Mhc, Myo10A, α-Spec, Kst), have axonal functions (e.g., Shot,
251 Dhc64C, Kst, Prosap), or scaffolding functions (Shot, Prosap). Consistent with similar results
252 in vertebrates (74), these results show that there is a clear overlap between the Top3β and
253 the FMRP activities but, additionally, the two proteins perform activities independent of the
254 other one.

255

256 **Top3β supports expression and subcellular localization of its transcript targets**

257 The *Top3β*^{Y332F} and *Top3β*^{26} mutants have reduced or no function, but the mutations cause
258 neither lethality nor sterility. This is a common phenomenon observed with conserved genes
259 and proteins that are still important for optimizing cellular physiology. In a lab setting, the
260 reduced function of these mutants can often be compensated for by other mechanisms.
261 However, by directly analyzing the cellular phenotypes of the mutants, one may observe
262 increased cellular stress and changes in physiology or anatomy that reveal the cellular
263 function of the normal gene. Such cellular stress and changes often lead to signs of premature
264 aging, like a decline in neuromuscular performance and a shorter lifespan.

265 To evaluate the consequences of the interaction of Top3β with its RNA targets, we selected
266 *shot*, *Dhc64C*, and *kst* from the top list of RNAs covalently bound to Top3β for further analysis.
267 These RNAs exhibit several distinctive features, including a high number of transcript
268 isoforms, long mRNAs, localized mRNAs, and maternal expression. Furthermore, their
269 homologs were also identified by a mammalian study (**Fig. 3**; (1)) and they are expressed in
270 neurons (22)(23). In normal young embryos, *shot* mRNA accumulates more strongly in the
271 polar granules and the pole cells at the posterior end (**Fig. 4)**. In embryos that were maternally
272 and zygotically mutant for *Top3β*, *shot* mRNA levels were overall reduced and the more
273 intense, localized staining pattern in the posterior pole region was lost in the null- and the
274 enzymatic $Top3\beta^{Y332F}$ mutant, but not in $Top3\beta^{\Delta RGG}$, suggesting that the normal expression
275 and localization depends on *Top3β* and particularly on its enzymatic activity. Analogous
276 studies revealed that the anti-Shot antibody signal was similarly weaker in the null mutant
277 and $Top3\beta^{Y332F}$ embryos compared to the wild type (**Fig. 4)**, suggesting that the reduced mRNA
278 levels caused the reduced Shot protein expression. These findings are consistent with *shot*
279 mRNA being the primary target of Top3β and they highlight the importance of the enzymatic
280 activity of Top3β for the efficient expression and localization of the encoded protein. In the
281 $Top3\beta^{\Delta RGG}$ mutant embryos, the Shot protein levels, and localization were less affected, like
282 the mRNA levels **(Fig. 4)**. The effects on the proteins encoded by two more *Top3β* targets
283 were similar. The cytoplasmic Dynein heavy chain (Dhc or Dhc64C) protein accumulated more
284 strongly at the posterior end of the wild-type embryo, in front of the pole cells. This was
285 neither detectable in the null mutant nor in $Top3\beta^{Y332F}$ **(Fig. 4)**. The Kst protein accumulated
286 at the apical cortex in normal blastoderm embryos, but in the *Top3β* null mutant and
287 $Top3\beta^{Y332F}$ its signal was reduced throughout the embryo, including the apical cortex. Protein
288 signals for Dhc and Kst showed an intermediate level in the $Top3\beta^{\Delta RGG}$ mutant embryos **(Fig.**
289 **4)**, indicating that the RGG box also affects their expression, albeit less strongly than the
290 catalytic activity.

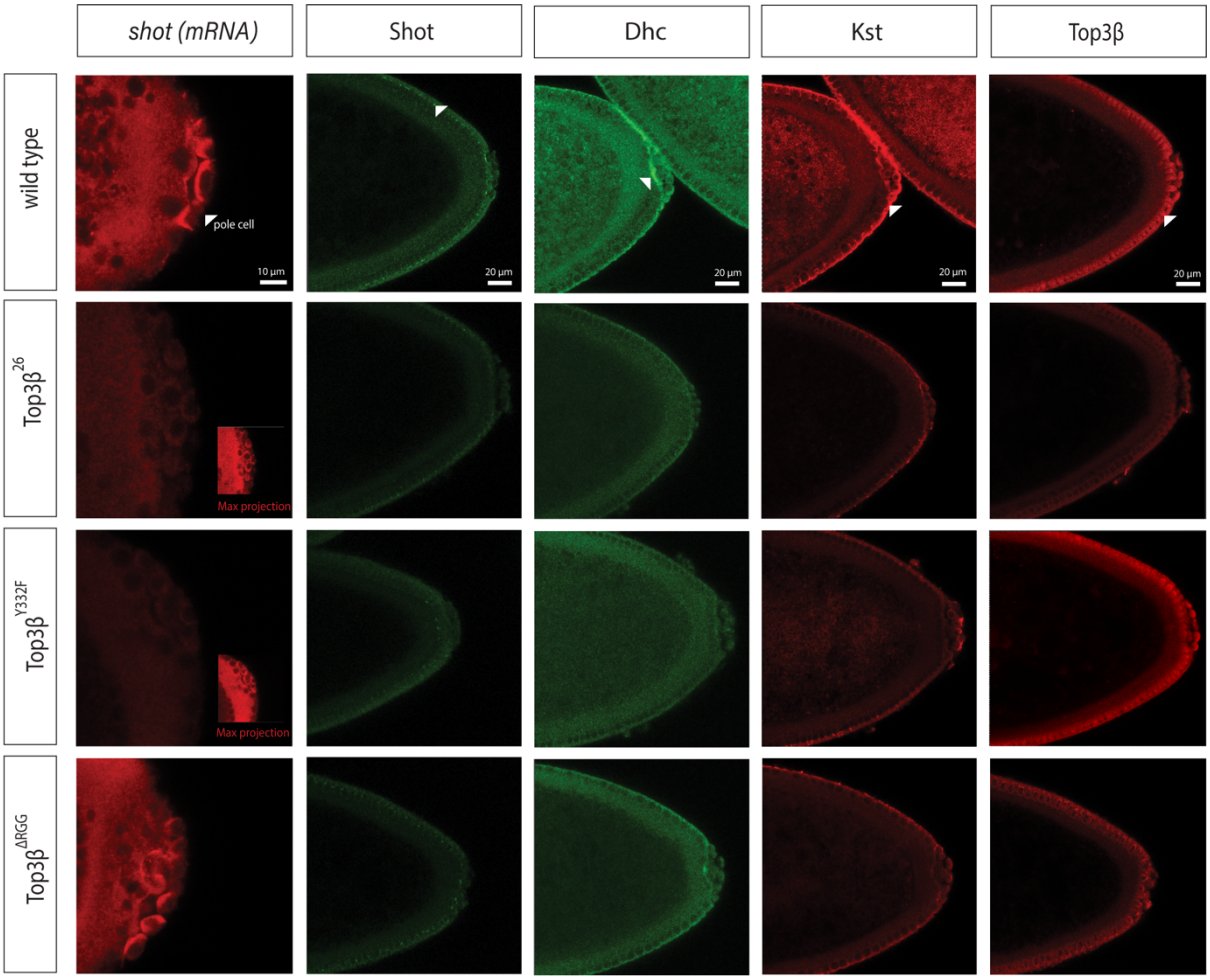

Fig. 4. Expression and localization of gene products of Top3β targets. The posterior pole of the embryos is shown to the right. *shot* mRNA and Shot protein localization in the posterior part of syncytial (*shot* mRNA) and cellularizing (Shot protein) wild-type embryos in the different *Top3β* mutants. Lower signal levels and less localized signals were seen in the null and *Top3β*^{Y332F}. Both were less reduced in *Top3β*$^{\Delta RGG}$ mutant embryos. Note the *shot* mRNA localization in the pole cells in the wild type and *Top3β*$^{\Delta RGG}$ mutant. Dhc64C localization at the posterior side of the somatic part of the embryo (arrowhead) was not detectable in the null mutant and *Top3β*^{Y332F} and reduced in *Top3β*$^{\Delta RGG}$ mutant embryos. Kst localization at the apical membrane (arrowhead) was reduced in null mutants and *Top3β*^{Y332F} compared to the wild type. Its localization was still identifiable in *Top3β*$^{\Delta RGG}$ mutant embryos. Top3β protein is localized similarly to its targets. It is, however absent from the null mutant which reveals the background level of the staining. Note also that Top3β is also nuclear in the wild type and *Top3β*^{Y332F}. Imaging settings were identical for the staining for the same protein and mRNA, respectively, in the different genotypes except for the insets which were overexposed to reveal the embryo. The scale bar is 10µm for the shot mRNA pictures and 20µm for the other micrographs.

Top3β normally localizes to the same area in blastoderm embryos as the different proteins and mRNAs described here. In the Discussion section, we will detail how this seems to contribute to an interesting gene expression mechanism. Note also that the wild-type protein and Top3β^{Y332F} localize to the cytoplasm and the nuclei **(Fig. 4)**. In contrast, Top3β$^{\Delta RGG}$ is clearly seen above background levels only in the cytoplasm. This indicates that its RGG box is needed

312 to localize Top3β to the nucleus and that the lack of the RGG box likely reduces the nuclear
313 functions of Top3β$^{\Delta RGG}$.

314

315 **Top3β supports neuronal structure and function in aging adults**

316 The negative geotaxis assay measures the activity of the nervous system and the muscles, and
317 the coordination between them. In this assay, all four *Top3β* genotypes showed similar
318 climbing abilities in young flies **(Fig. 5A).** Neuromuscular conditions sometimes become only
319 apparent at an older age because the young nervous system can compensate for some cellular
320 deficits. But such compensations can take their toll if they stress the cells. We, therefore,
321 tested for premature aging and age-related degeneration of the climbing ability. Indeed, as
322 seen in **Fig. 5A,** from week 6 on, the *Top3β*^{Y332F} and *Top3β*^{26} flies became slower, and their
323 climbing ability declined more than the wild-type one. The results suggest that Top3β plays a
324 role in aging and combating neurodegeneration in *Drosophila* motor neurons.

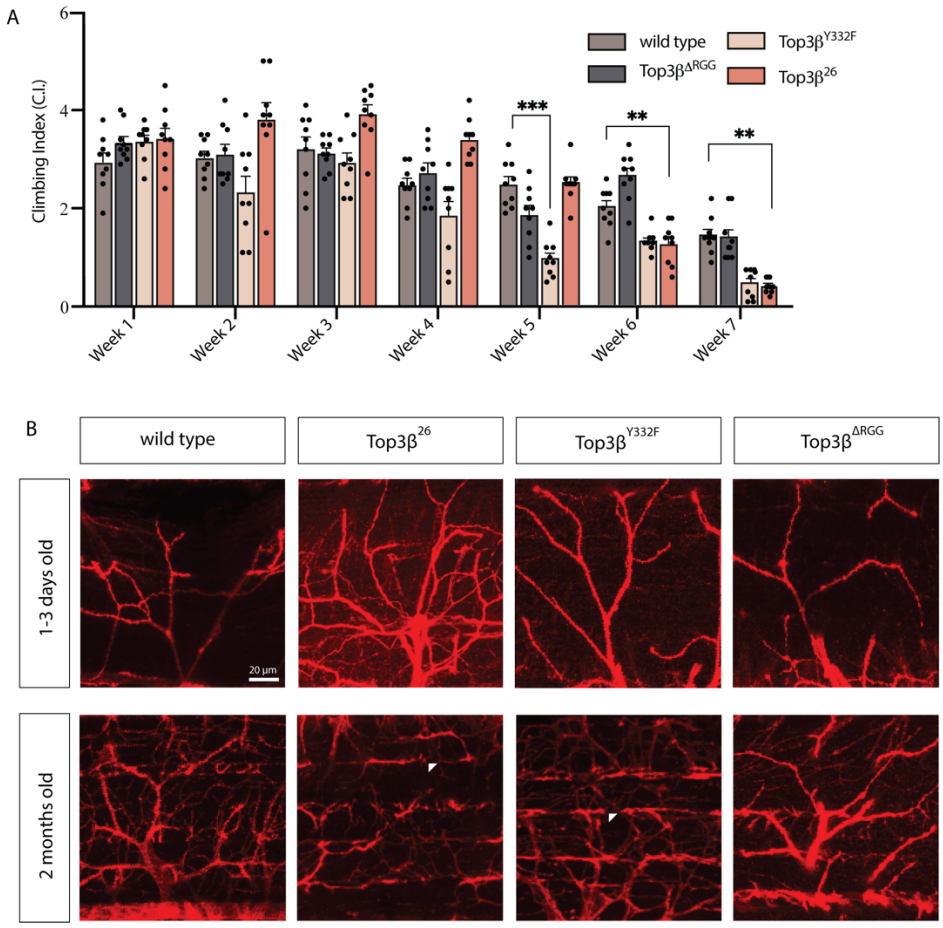

325

326 **Fig. 5: Aging effects of *Top3β* mutants. A)** Climbing assays of wild type, *Top3β*$^{\Delta RGG}$, *Top3β*^{Y332F}, and
327 *Top3β*^{26} flies. A two-way ANOVA analysis was performed. The graph bars show the mean climbing
328 index (C.I.) for the different genotypes. Error bars represent the standard error of the mean (S.E.M).
329 Each dot represents a calculated individual C.I. The adjusted p-values for each significant difference
330 are indicated on the graph. (p-value <0.0001=****, p-value <0.001=***, p-value <0.01=**, p-value
331 <0.05=*.) **B)** In adults, null mutant NMJs contain more branches than the wild type, indicative of a
332 compensatory mechanism. Arrowheads point to the lost synaptic integrity of the dorsal longitudinal flight
333 muscle (DLM). NMJ synapses were visualized by staining motor neurons with anti-HRP antibodies. The
334 progressive denervation of the DLM is particularly evident in the null and the *Y332F* mutant in the adult
335 thoracic NMJs. The scale bar represents 20μm. All panels show maximum intensity projections with a
336 z-step size of 0.7μm.

337

338 As the flies age, their motor abilities and neurotransmission decline, and fragmentation of
339 synaptic motor terminals becomes apparent (24). To gain insights into the possible adaptation
340 of the adult neuromuscular system, we also studied the structure of the adult neuromuscular
341 junctions (NMJs) in the four genotypes during aging **(Fig. 5B)**. Particularly the young null
342 mutants contained more branched structures compared to the simpler branch structures in
343 the wild type. Although to a lesser degree, young *Top3β*^{Y332F} and *Top3β*$^{\Delta RGG}$ mutants also
344 displayed presynaptic overgrowth. In older flies, premature loss of locomotive ability, a sign
345 of faster aging, became apparent in both *Top3β*^{26} and *Top3β*^{Y332F} flies by week 6 **(Fig. 5).**
346 Concomitant with this, denervation of the DLM (Dorsal Longitudinal Muscle) synapses
347 became evident. Particularly in the null mutants and also in *Top3β*^{Y332F}, loss of synaptic
348 integrity was observed during aging in 1-2 months old adult flies **(Fig. 5B)**. Because *Top3β*^{26}
349 and *Top3β*^{Y332F} flies live less long than wild-type and *Top3β*$^{\Delta RGG}$ flies **(Supplementary Fig. S4)**
350 and only living flies were selected for the NMJ preparation, the decline of their NMJ structure
351 and function is most likely even stronger than observed in living animals.

352 Even though the lack of *Top3β* activity seems to be compensated early on, we conclude that
353 loss of *Top3β* over extended periods leads to loss of synaptic integrity, faster aging, and
354 shortened lifespan. Given that lack of enzymatic activity of Top3β affects the expression of
355 many genes whose mRNAs are direct Top3β targets, it appears that reduced expression of
356 many genes can be compensated initially by the cells for some time and that these
357 compensations induce cellular stress that leads later to premature aging of the nervous
358 system and reduced neuromuscular performance.

359

360 ***Top3β* mutants enhance (G4C2)$_{49}$-induced neuronal toxicity in flies**

361 To gain deeper insights into the cellular significance of Top3β's catalytic activity toward one
362 specific RNA, we investigated its effect on the phenotype induced by GC-rich repeat RNA
363 sequences. For this, we used the repeat sequence (GGGGCC)$_{49}$ (also named G4C2)$_{49}$ that
364 induces neurotoxic effects in both humans and flies. In humans, the presence of 20-28 repeats
365 of this sequence was shown to be associated with neurodegenerative diseases such as
366 amyotrophic lateral sclerosis (ALS) and frontotemporal dementia (FTD) (25)(26)(27). Using a
367 GMR-GAL4 driver (28) to study the effect of this RNA on the adult eyes revealed that *Top3β*
368 mutants enhanced the neurotoxic effect of the (G4C2)$_{49}$ transcripts in the eyes of young flies
369 aged 1-2 days (**Fig. 6**). Of the *Top3β* mutants, *Top3β*^{26} and *Top3β*^{Y332F} exhibited the most
370 severe eye lesions with irregular ommatidial structures, and this was particularly evident from
371 the widespread cell death. Young *Top3β*$^{\Delta RGG}$ mutants displayed irregular ommatidia but
372 usually less cell death. After one month, the rough eye phenotype caused by the *Top3β*^{26} and
373 *Top3β*^{Y332F} mutants affected the entire eye, indicating widespread degeneration of
374 ommatidial cells. These results show that the topoisomerase activity of Top3β counteracts
375 the toxic activity of the (G4C2)$_{49}$ transcripts in the Drosophila model for this disease **(Fig. 6)**.

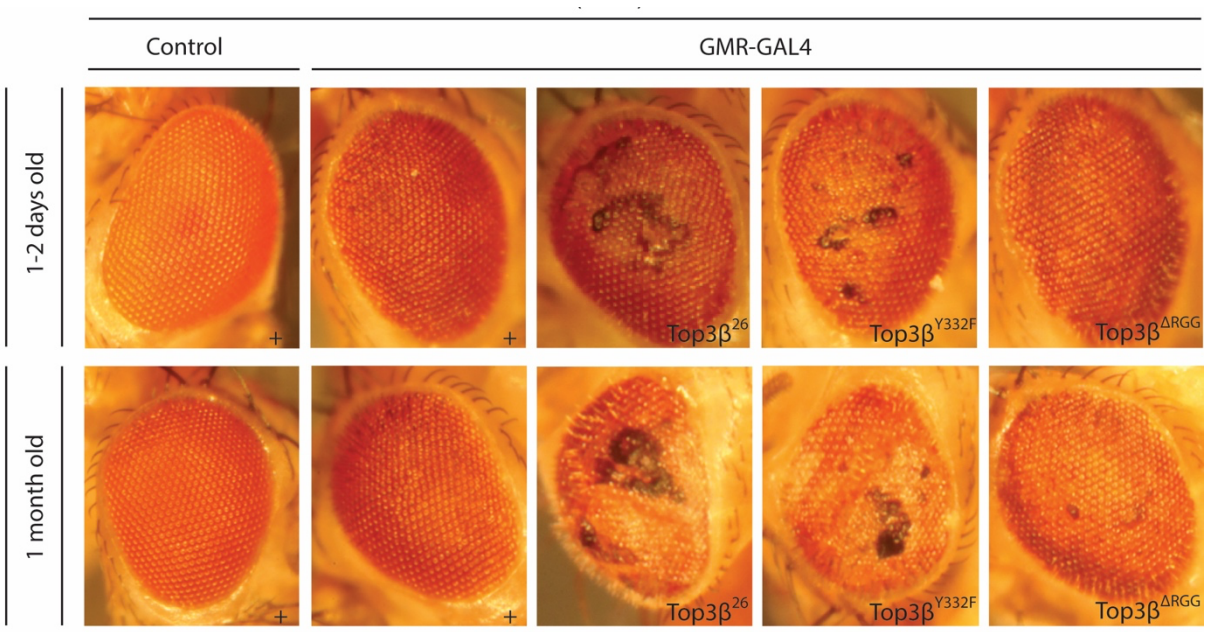

376

377 **Fig. 6: *Top3β* activities toward (G4C2)$_{49}$ repeat RNAs in the eye.** Expression of the UAS-(G4C2)$_{49}$
378 transgene in wild-type (+) and *Top3β* mutant flies using the GMR-GAL4 driver. *Top3β*$^{\Delta RGG}$ caused mild
379 disruptions, the *Top3β*^{26} and *Top3β*^{Y332F} mutants caused strong degeneration. Shown are data from
380 one experiment carried out in parallel; data were reproduced in a total of three or more independent
381 experiments. All *Top3β* mutants enhanced the degenerative phenotype of the (G4C2)$_{49}$ RNA.

382 Genotype: *Top3β*^{26} (or *Top3β*^{Y332F} or *Top3β*$^{\Delta RGG}$);;UAS-(G4C2)$_{49}$/GMR-GAL4. GMR-GAL4 control
383 genotype: *Top3β*$^{+}$; ;UAS-(G4C2)$_{49}$/GMR-GAL4.

384

385 **Discussion**

386 Top3β and its catalytic activity have a strong effect on the production of normal expression
387 levels of a considerable number of RNAs during embryonic development. Particularly long
388 pre-mRNAs and RNAs with long ORFs and long UTRs depend on *Top3β* for their normal
389 expression levels (**Fig. 1; Fig. 4**). This supports the hypothesis that to be expressed at proper
390 levels and locations, long RNA molecules are more dependent on RNA topoisomerases that
391 can solve structural problems. Longer ORFs increase the risk of stalling translation because
392 structural problems of the mRNA can prevent it from entering the ribosome. In such cases,
393 Top3β can rescue the translation of stalled mRNAs (74). UTRs contain elements that regulate
394 posttranscriptional gene expression like RNA localization and translational control (29) and
395 long 3'UTRs are a characteristic of mRNAs that are under these posttranscriptional controls.
396 RNAs with such long UTRs depend more strongly on *Top3β,* suggesting that localized and
397 translationally controlled mRNAs also depend more strongly on Top3β for their proper
398 expression. Indeed, the expression of three of the top targets of Top3β depended heavily on
399 *Top3β* in terms of expression levels and localization within the cell (**Fig. 4**).

400 RNA localization combined with translational control is a mechanism to provide local
401 expression of gene products and it is most important in large cells, but also for fine-tuning
402 gene expression in general. In support of this notion, *Top3β* mutations were implicated
403 specifically in several neurological diseases and cancers. The (pre)mRNAs that depend on
404 *Top3β* for normal expression in Drosophila embryos <u>and</u> whose homologs have been
405 implicated in one of the neuronal diseases or cancers are particularly long. This supports the
406 view that large RNAs depend more strongly on *Top3β.* Very likely because their length,
407 transport, and translational control provide strong risks for the inactivation of the RNA due to
408 structural problems. It is, therefore, evident that failure to rescue such RNAs in neuronal cells
409 interferes with the timely and local expression of the encoded proteins involved in neural
410 development, axonal growth, synaptic physiology, and plasticity.

411 The characteristics of the targeted RNAs suggest that Top3β is particularly involved in
412 processes like RNA localization, interactions with RNP particles, translation and its control,
413 and splicing. The protein interaction map **(Supplementary Fig. S3)** supports this
414 interpretation and further suggests that it might also be involved in RNA degradation**.**

415 ***RNA targets of Top3β***

416 Finding that Top3β interacts with splicing factors **(Supplementary Fig. S3; Table S5)** appears
417 to be a significant result because Top3β's RNA targets have a greater number of exons, longer
418 introns, and alternative transcripts **(Fig. 3)**. The fact that these parameters correlate with one
419 another (30)(31)(32)(33)(34) further strengthens the conclusion that Top3β participates in
420 the nuclear activity of RNA splicing. Moreover, snoRNAs are also enriched in the Top3β targets
421 and they play roles in mRNA splicing and editing and they are also involved in stress response
422 and metabolic homeostasis (35), two additional characteristics of Top3β targets
423 **(Supplementary Fig. S3; Tables S4,S5)**. The analysis of the *Top3β*$^{\Delta RGG}$ phenotype revealed that
424 the RGG motif is needed for the nuclear localization of a large fraction of Top3β in the
425 blastoderm embryo **(Fig. 4)**. The failure of the Top3β$^{\Delta RGG}$ mutant protein to localize to the
426 embryonic nuclei suggests that reduced nuclear functions of Top3β$^{\Delta RGG}$ might contribute to
427 the *Top3β*$^{\Delta RGG}$ mutant phenotype, too. This allele might therefore also become useful to
428 analyze the nuclear roles of *Top3β* in the future.

429 Longer pre-mRNAs pose not only more chances for splicing errors (because of the increased
430 difficulty in identifying the correct splice sites) but also for entanglement of the RNA. The
431 latter is also a considerable problem during transport over extended distances, which might
432 even involve mRNA packaging and unpackaging before the mRNAs can be activated for
433 translation at the right place and at the right time. During such transport, extended molecules,
434 such as mRNAs, stand an increased chance of becoming entangled or suffering other
435 structural problems that might interfere with their transport or translation. The coding
436 sequence (CDS) and untranslated regions (UTRs) of an mRNA molecule are also important for
437 regulating gene expression at the level of RNA localization and translation. Particularly 3'UTRs
438 affect not only the translation in neurons but also the localization to the places where these
439 mRNAs will be translated in response to extrinsic stimuli, such as neurotrophins, synaptic
440 activation, and regeneration after injury (36)(8)(37)(38). Consistent with the proposed
441 function of Top3β in rescuing (pre-)mRNAs with the described characteristics, the embryonic
442 targets of Top3β displayed a strong bias for these characteristics (**Fig. 3; Supplementary**
443 **Tables S4,S5**) and the enzymatic activity of *Top3β* is particularly important for mRNAs that
444 are generated from long pre-mRNAs, for mRNAs with long 3'UTRs and those with long coding
445 sequences (**Figs. 1B-D; Supplementary Table S1**). These mRNAs are expressed at reduced

446 levels in the absence of the RNA topoisomerase activity and mRNAs with these characteristics
447 were found to bind to Top3β.

448 ***Important targets of Top3β***

449 The normal expression levels of the *Ras opposite* (*Rop)* mRNA in young Drosophila embryos
450 depend on *Top3β* (**Fig. 2C**; **Supplementary Table S1**). In the context of human neurological
451 diseases, this was particularly striking because the human homolog of *Rop* is differentially
452 expressed in all neurological diseases with which human *Top3β* had been associated **(Fig. 2C)**.
453 *Rop* mRNA was also identified as a significant direct target of Top3β with an adjp-value of
454 0.027 **(Supplementary Table S3).** *Rop* regulates neurotransmitter secretion in a dosage-
455 dependent manner (6) and it has been described to act in synaptic vesicle priming and
456 transport. In *Rop* mutants, the release of neurotransmitters from the pre-synapse area into
457 the synaptic cleft fails to occur. It, therefore, seems that *Rop* could be a rewarding gene to
458 further investigate.

459 Localization of mRNAs combined with translational control is a mechanism that is particularly
460 important in large cells (like oocytes and young embryos) and cells with large extensions (like
461 neurons). Many of the identified mRNAs function in these cells and have important roles in
462 neurons because they encode large cytoskeletal and cortical elements (e.g., *kst*, *α-spec*, *shot,*
463 *mgl*) or regulators of NMJ growth (e.g., *Prosap*). An interesting Top3β target is the *shot* mRNA,
464 which had been identified as a Top3β target in Drosophila and mammals, and also as an FMRP
465 target in mammalian cells (**Fig. 3F**; (1)(74)). In Drosophila, normal *shot* mRNA levels also
466 depend on *Top3β* and its enzymatic activity (**Supplementary Tables S3,S4; Fig. 4**). *shot*
467 encodes a spectraplakin family member, a large cytoskeletal linker molecule that binds actin
468 and microtubules and participates in axon growth and neuromuscular junction maintenance
469 and growth control (39),(40),(41),(42). Drosophila *shot* has additional roles in many other
470 tissues and cell types and it consists of 45 exons producing 22 transcript isoforms, which is
471 many more than the average of 2 isoforms per *Drosophila* gene. *shot* RNA and protein
472 expression in embryos are markedly reduced and less localized in *Top3β* null mutants and in
473 the enzymatically dead $Top3\beta^{Y332F}$ embryos (**Fig. 4**). The enzymatic activity of Top3β is
474 therefore key to the proper expression of *shot* mRNA and protein. The reduced *shot* mRNA

475 levels and localization might reflect a role of Top3β in splicing *shot* pre-mRNAs, in localizing
476 *shot* mRNA, and in resolving RNA entanglements.

477 Along with α-Spec, Kst (β_H-Spectrin) crosslinks F-actin and acts as a molecular scaffold when
478 it is recruited to the apical membrane of epithelial cells (43)(44). The mRNAs encoding these
479 two proteins are both targets of Top3β, and we showed that the normal expression levels and
480 localization of the Kst protein in the embryos depend on the enzymatic activity of Top3β,
481 suggesting that the lack of Top3β affects Kst protein production at the level of *kst* mRNA
482 production, localization and/or translation. Interestingly, Top3β accumulates also
483 preferentially at the apical cortex of embryos, further suggesting that higher Top3β activity in
484 this location may contribute to the apical translatability of apical transcripts – for instance by
485 rescuing entangled mRNAs -, thereby expressing the encoded protein in this location at higher
486 levels, even if the mRNA is uniformly expressed. It thus appears that subcellular localization
487 of Top3β activity might serve as a novel tool to target gene expression to specific cellular
488 locations even for mRNAs that are expressed uniformly.

489 Being the major retrograde cytoplasmic motor in all cells, neuronal cytoplasmic dynein moves
490 cargo from the synapse along the axon and back to the cell body (45). During Drosophila
491 oogenesis, dynein transports mRNAs, proteins, and organelles from the nurse cells into the
492 oocyte, where they are deposited for the young embryo. In the embryo, it then transports
493 them to the apical cortex (76)(77). The apical accumulation of the large Dynein heavy chain
494 (Dhc) subunit of the cytoplasmic dynein complex (75), depends heavily on *Top3β* (**Fig. 4**).
495 Both null and *Top3β*^{Y332F} embryos showed reduced Dhc protein staining and lack of Dhc
496 concentration at the apical cortex. Top3β and its enzymatic activity act on the *Dhc* mRNA and
497 this is needed to allow proper Dhc protein expression and polar distribution. Possibly pointing
498 to a feedback effect, Top3β also forms a complex with FMR1 (1), which binds to the cargo
499 adaptor BicD of the dynein transport machinery (46), which can localize its cargo at the apical
500 cortex.

501 ***Top3β environment and relevance***

502 The enrichment of neuronal and other ribonucleoproteins (RNP) forming granules, was a clear
503 result of the analysis of the Top3β interactors (**Supplementary Fig. S3A**). In the case of the
504 neuronal RNP granules, they concentrate specific sets of mRNAs and regulatory proteins in

505 the same location, promoting their common long-distance transport to axons or dendrites
506 (20)(21). They also have a dual function in regulating the translation of associated mRNAs
507 (47). As a component of neuronal RNPs, Me31B mediates the transport and controls the
508 translation of neuronal RNAs, including the translational repression of synaptic transcripts
509 (26). We found Me31B highly enriched with Top3β and this interaction depended on the RGG
510 box, suggesting that the RGG box links Top3β to the neuronal RNPs.

511 Consistent with our analysis of physically interacting proteins (**Supplementary Fig. S3; Table**
512 **S5**), Top3β had already been described to be present in complexes with FMR1 (1). Comparing
513 the datasets of significantly less abundant transcripts in the extracts of *Top3β* mutants
514 (**Supplementary Table S1**) to the data of significantly less translated transcripts upon *Fmr1*
515 RNAi treatment in Drosophila ovaries (48) revealed many shared mRNAs (**Fig. 7)**. Even though
516 different tissues have been used for the two experiments, a large fraction of the ovarian
517 transcripts end up in the young embryo. The overlap between the two data sets indicates that
518 FMR1 and Top3β proteins act on many of the same mRNAs, but that *FMR1* and *Top3β* are
519 also involved in additional functions independently of each other.

A

shared targets in Fmr1 and downregulated RNAs in embryo			
PCB	spir	shi	spri
svr	Atpalpha	Mrtf	Hsc70-3
spen	CG10960	mld	CG31729
oys	toc	Exn	Ack-like
Abl	raskol	Ptp99A	BicD
Glut1	Med	Pde11	Nost
CG43783	Dys	fs(1)h	ctrip
slif	Crag	CG2747	CG13917
Mbs	mtd	stx	SP1029
cnc	CG2818	cana	

B

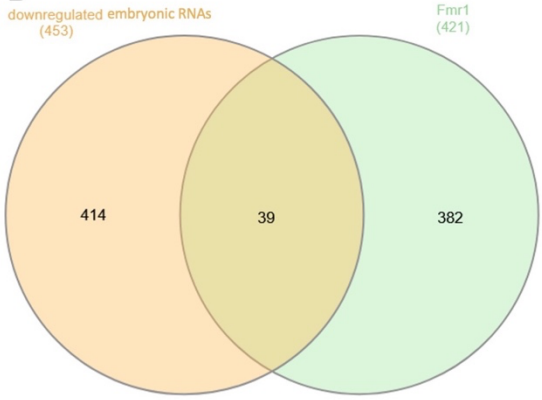

520
521 **Fig. 7.** Ovarian mRNAs depending on *FMR1* for their translation and on *Top3β* for their normal
522 accumulation in young embryos. **A)** List of the shared mRNAs and **B)** Venn diagram of the
523 overlap between the two datasets.
524
525
526 The lack of RNA topoisomerase activity can interfere with the expression of many different
527 genes involved in a variety of different pathways. The resulting suboptimal functioning of
528 different cellular mechanisms is likely to interfere with cellular physiology, making it less
529 efficient and producing cellular stress. Further research needs to test, which of the individual

530 pathways suggested by our work causes a physiological problem in the human conditions
531 involving *Top3β*. Serious neurological health issues often arise when several pathways are not
532 functioning properly anymore, making it difficult to pinpoint a single primary cause. Our work
533 revealed that reduced activity of Top3β affects several of the pathways that rely on mRNAs
534 that are Top3β targets. The combination of defects in different physiological pathways is likely
535 to impact the outcome of the various neurodevelopmental and cognitive disorders and
536 cancers with altered *Top3β* function.

537

538 ## Material and Methods

539 ### Fly stocks and maintenance

540 The *white* (*w)* strain was used as a wild-type control as this was the genetic background of the
541 mutants used in this study. The mutant fly stocks *Top3β*^{Y332F} and *Top3β*$^{\Delta RGG}$ were established
542 as described below. *Top3β*^{26} was from Lee and colleagues (49). The fly stocks were grown and
543 maintained on a regular corn medium (ingredients: corn, yeast powder, sucrose syrup, agar,
544 potassium sodium tartrate tetrahydrate, water, nipagin, and propionic acid) supplied with
545 brewer's yeast for the experiments. All *Drosophila melanogaster* fly stocks were stored at
546 18°C in glass or plastic vials with day/night (12 h/12 h) light cycles. All experiments were
547 performed at 25°C. $(G4C2)_{49}$ flies (Stock #84727; (28)) express 49 pure 5'GGGGCC3' repeats
548 under the control of UAS. These repeats are neurotoxic and model the G4C2 repeats seen in
549 human *C9orf72* that are associated with Amyotrophic Lateral Sclerosis and Frontotemporal
550 Dementia.

551

552 ### Generation of *Top3β* alleles

553 Genomic sequences were scanned for suitable sgRNA target sites with the JBrowse from
554 FlyBase and appropriate sgRNA sequences were chosen based on (a) their distance from the
555 tagging site, and (b) the absence of potential off-target sites on the same chromosome as the
556 target site (51). To mutate the endogenous *Top3β*, a sgRNA was designed, which hybridized
557 in the vicinity of the Y332 codon of *Top3β* and induced the Cas9 nuclease to perform a double-
558 strand break. Complementary oligodeoxynucleotides with suitable overhangs
559 (**Supplementary Table S6**) were annealed and cloned into the pCFD5 vector, which is used to
560 express the sgRNA (52). The Cas9 fly stock was obtained from the Bloomington Stock Center
561 (#79004). ssDNA was designed for the mutation changing the Tyr (Y) to a Phe (F) codon and
562 injected into the progeny produced by Cas9- and sgRNA-expressing flies. The single-strand
563 oligodeoxynucleotide with the flanking arms precisely matching the endogenous sequences
564 changes the sequence at the mutation site by serving as a template (**Supplementary Table**
565 **S6**) for the homologous recombination DNA repair at the double-strand break. The same
566 strategy was used to delete the endogenous RGG region in *Top3β* (ΔRGG) using the
567 appropriate gRNA and ssDNA templates.

568

569 **RNA sequencing**

570 RNA sequencing was performed using 1 mL of TRIzol® Reagent per 50-100 mg of tissue
571 samples (0-2 hours embryos and 1-5 days old heads), which were homogenized at room
572 temperature. RNA extraction was done according to the Trizol protocol. The University of
573 Bern's Next Generation Sequencing Platform conducted quality control assessments, library
574 generation, sequencing runs, and sequencing quality control steps. The purified total RNA was
575 assessed for quantity and quality using a Thermo Fisher Scientific Qubit 4.0 fluorometer with
576 the Qubit RNA BR or HS Assay Kit (Thermo Fisher Scientific, Q10211 or Q32855, respectively)
577 and an Agilent Advanced Analytical Fragment Analyzer System using a Fragment Analyzer RNA
578 Kit (Agilent, DNF-471), respectively. Sequencing libraries were made using a CORALL Total
579 RNA-Seq Library Prep Kit with UDI 12nt Set A1 (Lexogen, 117.96) according to Lexogen's
580 guidelines. The libraries were paired-end sequenced using either shared Illumina NovaSeq
581 6000 SP, S1, or S2 Reagent Kits (200 cycles; Illumina, 200240719, 2002831, or 20028315) on
582 an Illumina NovaSeq 6000 instrument. The quality of the sequencing runs was assessed using
583 the Illumina Sequencing Analysis Viewer (Illumina version 2.4.7), and all base call files were
584 demultiplexed and converted into FASTQ files using Illumina bcl2fastq conversion software
585 v2.20.

586 The quality and quantity of reads generated from RNA-seq were evaluated. Most of the reads
587 were from mature transcripts without introns, but we mapped them to the reference genome
588 that includes introns using an alignment tool like Hisat2 that can handle large gaps. This
589 required information on where each gene is located in the genome, available for example
590 from Ensemble (53). The number of reads mapping to each gene was counted using the
591 FeatureCounts tool, which requires information about the location of each gene in the
592 genome. This resulted in a table of read counts for each sample and gene.

593 To test for differential expression between two experimental groups containing three
594 biological replicates each, we used the DESeq2 tool. The analysis included the following steps:
595 1. Normalization to correct for differences in the total number of reads between samples. 2.
596 Variance estimation between replicates to account for the limited number of replicates in
597 RNA-seq experiments (DESeq2 incorporates information from other genes with similar overall

598 expression levels into the estimation). 3. Log-fold change (LFC) adjustment based on evidence
599 strength which was estimated by the LFC. If it is weak (e.g., because the gene is expressed at
600 low levels, the variance between replicates is high, or there are few replicates), the LFC shrinks
601 toward zero. 4. Calculation of a test statistic and comparison to the normal distribution to
602 obtain a p-value. 5. Multiple test corrections using the Benjamini-Hochberg procedure to
603 consider only potentially detectable, differentially expressed genes. DESeq2 applies a false
604 discovery rate correction based on the Benjamini-Hochberg procedure. However, the
605 multiple-test correction considers only genes that could potentially be detected as
606 differentially expressed. Only these genes will have an adjusted p-value. The mean read count
607 across all samples is used to decide if a gene should be included or not.

608

609 **Extracting transcript features**

610 The information about exon length, exon count, 3´UTR length, gene name, gene length, 5´UTR
611 length, mRNA length, and CDS length was extracted from the gtf file of dmel-all-filtered-
612 r6.42.gff using a custom python script.

613

614 **Generation of the *Top3β::eGFP* cDNA clone for GAL4>UAS expression**

615 For the *Top3β::eGFP* construct, the *Top3β* cDNA clone LD10035 was amplified. Enhanced GFP
616 (EGFP) was PCR amplified from a plasmid (pEGFP–C3). PCR amplified fragments were run on
617 an agarose gel and purified using the Wizard SV kit (Promega). The sequences were cloned
618 into the pUASz1.0 vector (54) with the *eGFP* ORF at the C-terminal end of the *Top3β* ORF using
619 a ligation kit (NEB). The UASz vector allows one to induce the constructs in any tissue,
620 including the somatic tissue, the germline, and the CNS (54). Plasmids were sequenced to
621 confirm the integrity of the construct and purified with a PureYield kit (Promega) for injection.
622 Transgenic stocks were established with the attP landing platform 86F from the Bloomington
623 Stock Center (#24749).

624 To generate an enzymatically dead enzyme, a Phe codon substituted the codon for the Tyr
625 responsible for crosslinking the enzyme with the nucleic acid in the *UASz- Top3β::eGFP* vector
626 to give rise to *UASz- Top3β^{Y332F}::eGFP*. Similarly, to figure out the role of the RGG box, we

627 deleted in the *UASz- Top3β::eGFP* vector the sequence coding for this box, giving rise to *UASz-*
628 *Top3β$^{\Delta RGG}$::eGFP*. At the site of the desired mutation, oligonucleotide primers with the
629 desired mutation were used to amplify the mutant double-stranded DNA plasmid
630 (**Supplementary Table S6)**. A protocol based on two different PCR amplifications was used for
631 this. First, two elongation reactions were carried out, with one of the two primers each. In
632 the second reaction, the two initial elongation reactions were mixed and an additional PCR
633 reaction was carried out. The wild-type and mutant eGFP fusion constructs were transformed
634 into *Drosophila* using the attP-86F landing platform. mat-tub-GAL4 (#7062) was used to drive
635 the expression in the older female germline and GAL4-BG380 (#24749) to drive expression in
636 the CNS. UASz-eGFP transgenic flies, obtained from the Bloomington stock center, were used
637 as negative controls.

638

639 **Sample preparation for mass spectrometry**

640 Drosophila Top3β::eGFP was purified using the GFP tag and a mouse anti-eGFP antibody as
641 described previously (55). Protein G magnetic beads were washed 3x with PBS and incubated
642 for 2 hours with an anti-GFP antibody. After this, they were washed 3x with 1 ml 1x PBS and
643 one more time with 1 ml homogenization buffer (25 mM Hepes PH 7.4; 150 mM NaCl; 0.5
644 mM EDTA PH 8.0, 1 mM DTT, protease inhibitors). To prepare the extracts, 1 ml
645 homogenization buffer was added to 1 gr of the samples (dechorionated embryos 0-2 hours
646 or adult heads 1-5 days old) in the glass homogenizer. The samples were homogenized and
647 transferred into the tube. Homogenized samples were centrifuged at 16,000 g (RCF), 4°C for
648 40 min. The interphase was transferred into a fresh Eppendorf tube, centrifuged again at
649 16,000 g, 4°C for 40 min, and transferred into a fresh tube. Beads were then incubated with
650 the extracts for 6 hours at 4°C on a wheel and the extracts were subsequently removed from
651 the beads. The beads were washed once with 1 ml homogenization buffer and then several
652 times with wash buffer (25 mM Hepes PH 7.4; 150 mM NaCl; 0.5 mM EDTA PH 8.0; 1 mM DTT;
653 protease inhibitors). The wash buffer was removed, and the beads were sent for mass
654 spectrometry.

655

656 **Mass spectrometry**

657 Mass spectrometry analysis was done by the Proteomics and Mass Spectrometry Core Facility
658 of the University of Bern, and the data are available in **Supplementary Table S5**. Proteins in
659 the affinity pull-down were re-suspended in 8M Urea / 50 mM Tris-HCl pH8, reduced for 30
660 min at 37°C with 0.1M DTT / 100 mM Tris-HCl pH8, alkylated for 30 min at 37°C in the dark
661 with IAA 0.5M / 100 mM Tris-HCl pH8, dilute with 4 volumes of 20 mM Tris-HCl pH8 / 2 mM
662 CaCl2 before overnight digestion at room temperature with 100 ng sequencing grade trypsin
663 (Promega). Samples were centrifuged, and a magnet holder trapped the magnetic beads to
664 extract the peptides in the supernatant. The digests were analyzed by liquid chromatography
665 (LC)-MS/MS (PROXEON coupled to a QExactive mass spectrometer, ThermoFisher Scientific)
666 with three injections of 5 µl digests. Peptides were trapped on a µPrecolumn C18 PepMap100
667 (5 µm, 100 Å, 300 µm×5 mm, ThermoFisher Scientific, Reinach, Switzerland) and separated
668 by backflush on a C18 column (5 µm, 100 Å, 75 µm×15 cm, C18) by applying a 60 min gradient
669 of 5% acetonitrile to 40% in water, 0.1% formic acid, at a flow rate of 350 ml/min. The Full
670 Scan method was set with a resolution at 70,000 with an automatic gain control (AGC) target
671 of 1E06 and a maximum ion injection time of 50 ms. The data-dependent method for
672 precursor ion fragmentation was applied with the following settings: resolution 17,500, AGC
673 of 1E05, maximum ion time of 110 milliseconds, mass window 2 m/z, collision energy 27,
674 underfill ratio 1%, charge exclusion of unassigned and 1+ ions, and peptide match preferred,
675 respectively.

676 The data were then processed with the software MaxQuant (56) version 1.6.14.0 against the
677 UniProtKB(57) Drosophila 7228 database (release 2021_02) containing canonical and isoform
678 entries, to which common contaminants were added. The following parameters were set:
679 digestion by strict trypsin (maximum three missed cleavages), first search peptide tolerance
680 of 15 ppm, MS/MS match tolerance of 20 ppm, PSM and protein FDR set to 0.01 and a
681 minimum of 2 peptides requested per group. Carbamidomethylation on cysteine was selected
682 as a fixed modification; the following variable modifications were allowed: methionine
683 oxidation, deamidation of asparagines and glutamines, and protein N-terminal acetylation; a
684 maximum of 3 modifications per peptide was allowed. Match between runs was turned on
685 (match time windows 0.7 min) but only allowed within replicates of the same kind.

686 Peptides were normalized by variance stabilization (58), imputed and combined to form Top3
687 (59) intensities, and considered alongside MaxQuant's Label-Free Quantification (LFQ) values.
688 Missing peptides, respectively LFQ intensities, were imputed by drawing values from a
689 Gaussian distribution of width 0.3 centered at the sample distribution mean minus 2.5x the
690 sample standard deviation, provided there were at most 1 non zero value in the group;
691 otherwise, the Maximum Likelihood Estimation (60) was used. Differential expression was
692 performed by applying the empirical Bayes test (61) between groups; significance testing was
693 performed as described (62).

694

695 **RNA immunoprecipitation**

696 Protein G magnetic beads were washed 2-3x with 1ml blocking buffer (20 mM Hepes, 150
697 mM KCl, 20% Glycerol, 0.5 % Tween, BSA (Biolabs), Heparin 0.2 mg/ml, SDS 0.1%, 1/2 pill EDTA
698 free protease inhibitors). Beads were blocked with a blocking buffer for 2-3 hours at room
699 temperature. An anti-GFP antibody was added to the beads and rotated for 1-2 hours. Beads
700 were washed 3x with non-hypotonic lysis buffer (20 mM Hepes, 1 mM EDTA, 150 mM KCL, 1
701 mM DTT, 0.5% Tween, 20% glycerol, SDS 0.1%, 1/2 pill EDTA free protease inhibitors). Anti-
702 GFP antibody was added to the beads and rotated for 1-2 hours at room temperature. Beads
703 were washed 3x with non-hypotonic lysis buffer.

704 Dechorionated embryos were 0-2 hours old. 1g of the embryos were homogenized in 2 ml
705 hypotonic lysis buffer (20 mM Hepes, 10 mM KCL, 1 mM EDTA, 1 mM DTT, 0.5% Tween, SDS
706 0.1%, 1/2 pill EDTA free protease inhibitors, and RNase inhibitor (Biolabs, 40,000U/ml)). 600
707 μl of extract, 323 μl of Adjusting buffer (57% Glycerol 100%, 0.4M KCl, 1 mM EDTA, 1 mM
708 DTT, 20 mM Hepes, SDS 0.1%), and 2 μl of RNase-free DNase I (20 μ/ml, Roche) were added
709 to the washed antibody beads and were precipitated ON rotating at 4°C. Samples were
710 washed 8x with 1 ml high salt wash buffer (20 mM Hepes, 1 mM EDTA, 200 mM KCl, 1 mM
711 DTT, 0.5% Tween, 20% Glycerol, SDS 0.1%, 1/2 pill EDTA free protease inhibitors, and RNase
712 inhibitor (Biolabs, 40,000U/ml)). On the last wash, 100 μl of the samples were taken before
713 centrifugation. 100 μl of proteinase K buffer, 1.5 μl proteinase K (20 mg/ml Roche), and RNase
714 inhibitors were added to each tube and were incubated for 30 minutes at 55ºC. 1 ml Trizol

715 reagent was added to each tube, and RNA was extracted according to the Trizol protocol
716 (TRIzol™ Reagent, Invitrogen™, Catalog number: 15596026).

717 The Next Generation Sequencing Platform, University of Bern, conducted quality control
718 assessments, library generation, sequencing runs, and sequencing quality control steps. The
719 quantity and quality of the purified total RNA were assessed using a Thermo Fisher Scientific
720 Qubit 4.0 fluorometer with the Qubit RNA BR or HS Assay Kit (Thermo Fisher Scientific,
721 Q10211 or Q32855, respectively) and an Advanced Analytical Fragment Analyzer System using
722 a Fragment Analyzer RNA Kit (Agilent, DNF-471), respectively. Sequencing libraries were made
723 using a CORALL Total RNA-Seq Library Prep Kit, Version 1 with UDI 12nt Set A1 (Lexogen,
724 117.96) according to Lexogen's guidelines for this kit. Pooled cDNA libraries were paired-end
725 sequenced using either shared Illumina NovaSeq 6000 SP, S1, or S2 Reagent Kits (200 cycles;
726 Illumina, 200240719, 2002831, or 20028315) on an Illumina NovaSeq 6000 instrument. The
727 quality of the sequencing run was assessed using Illumina Sequencing Analysis Viewer
728 (Illumina version 2.4.7) and all base call files were demultiplexed and converted into FASTQ
729 files using Illumina bcl2fastq conversion software v2.20.

730 The quality of the RNA-seq reads was assessed using fastqc v0.11.9 (63) and RSeQC v4.0.0
731 (64). Unique molecular identifiers (UMI) were extracted with umi-tools v1.1.2 (65), and
732 adapters were trimmed with cutadapt v3.4.1 (66) according to manufacturer instructions. The
733 reads were aligned to the Drosophila reference genome (BDGP6.32) using hisat2 v2.2.1 (67).
734 FeatureCounts v2.0.1 (68) was used to count the number of reads overlapping with each gene
735 as specified in release 103 of the Ensembl genome annotation. The Bioconductor package
736 DESeq2 v1.36.0 (69) was used to test for differential gene expression between the
737 experimental groups. To generate the log2 fold change versus transcript length plots, the
738 estimated log2 fold change per gene was plotted against the most extended transcript length
739 per gene with R v4.2.1 (70). We used the log2 fold change>=1 and the adjusted p-value (adjp-
740 value) <0.05 of enrichment over control for further analysis.

741

742 **Dissection and immunostaining of adult Dorsal Longitudinal Muscles (DLMs)**

743 Thoraces of 0-3 days old and 2 months old adult wild-type, *Top3β*^{Y332F}, *Top3β*$^{\Delta RGG}$, and
744 *Top3β*^{26} flies were separated from the rest of the body in 1x PBS. The thoraces were fixed in

745 PFA (32% formaldehyde diluted to 4% with 1x PBS) for 30 min at room temperature and then
746 washed 3x with PBS. All 1x PBS was removed from the tubes using a Pasteur pipette. The
747 tubes were submerged into a liquid nitrogen flask for 10 seconds using cryogenic tweezers.
748 Then, 300 µL of ice-cold 1x PBS was added to the samples. The thoraxes were cut into two
749 hemithoraxes, transferred into 1x PBS (24), and blocked in 1x PBS with 0.1% normal goat
750 serum and 0.2% Triton X-100 at pH 7.4 for at least one h at 4°C. Mouse anti-HRP or anti-Brp
751 (nc82; 1:125 dilution) from Developmental Studies Hybridoma Bank were used to stain motor
752 neurons. Primary antibodies were removed on the following day and the tissue was washed
753 four times with PBST for 5 min each on a rotator. For the secondary antibody staining, goat
754 anti-mouse A647 (1.5 mg/ml, diluted 1:200 dilution; Jackson ImmunoResearch Laboratories
755 Inc.) was added to the samples, which were then kept at room temperature for 2 hours in a
756 dark box on the rotator. After the 2 h incubation, the secondary stain was washed out 4 times
757 for 5 min with PBST. Then, the samples were mounted on a slide (24).

758

759 **Negative geotaxis (climbing) assays**

760 Wild-type flies and the three *Top3β* mutant strains were reared on fresh food and allowed to
761 hatch at 25° C. For each genotype, all 0-3-day-old adult male flies were collected. Ten young
762 adult male flies, each, were anesthetized and placed in 4 separate graduated flat-bottom glass
763 cylinders. After 1 hour of recovery from CO_2 exposure, flies were gently tapped 4x to the
764 bottom of the cylinder to startle them repeatedly with constant force to displace the flies to
765 the bottom surface. The flies were then allowed to climb the wall until they reached the top
766 of the column. The climbing procedure was video recorded using an iPhone 11 Pro. These
767 assays were repeated every week over 7 weeks on the same weekday. Three fly batches, each,
768 provided the material for the triplicates which were performed within 5-minute intervals.
769 After the three trials, each batch of 10 flies was transferred into glass vials and kept at 25° C.
770 Before the experiment, every single batch was inspected to ensure that all 40 flies could be
771 video-tracked when they started to climb after the tapping. To calculate each climbing index
772 (CI), flies that remained at the bottom were counted as in zone 0. The formula used to
773 calculate the CI is CI = (0 x n0 + 1 x n1 + 2 x n2 + 3 x n3 + 4 x n4 + 5 x n5) / nTotal, where nTotal
774 is the total number of flies and nx is the number of flies that reached zone x.

Statistics

All statistical analyses were performed using GraphPad Prism 8. For the negative geotaxis assays, the means, standard error of the means, and p-values were obtained by two-way ANOVA with Tukey's multiple comparison test.

Acknowledgments

Our thanks go to P. Nicholson and the members of the University of Bern NGS platform for sequencing the many RNA samples and to the IBU group of R. Bruggmann, particularly, S. Oberhänsli and G. van Geest, for their important support during the analyses of the sequencing data. We thank the University of Bern (Switzerland) Mass Spectrometry Center (PMSCF) members S. Braga Lagache and N. Buchs for performing the MS experiments and M. Heller and A-C. Uldry for the data analysis. We wish to acknowledge all our group members who gave their time and expertise to provide critical input and technical support. Special thanks go to P. Vazquez, R. Dörig, and D. Beuchle. We highly appreciate the continuous support from friends and colleagues in the fly community for sharing their results, fly stocks, and antibodies. For this work, too, FlyBase provided invaluable support, the Developmental Studies Hybridoma Bank provided antibodies, and the Bloomington Drosophila Stock Center (NIH P40OD018537) fly stocks.

Funding

This work was supported by the Swiss National Science Foundation project grants 31003A_173188 and 310030_205075 and by the Equipment grant 316030_150824 to BS. Support came also from the University of Bern to BS. The funders had no role in study design, data collection, and interpretation, or the decision to submit the work for publication.

801 **References**

802 1. Xu D, Shen W, Guo R, Xue Y, Peng W, Sima J, et al. Top3β is an RNA topoisomerase
803 that works with fragile X syndrome protein to promote synapse formation. Nat
804 Neurosci. 2013;16(9):1238.

805 2. Ahmad M, Shen W, Li W, Xue Y, Zou S, Xu D, et al. Topoisomerase 3β is the major
806 topoisomerase for mRNAs and linked to neurodevelopment and mental dysfunction.
807 Nucleic Acids Res. 2017;45(5):2704–13.

808 3. Kaufman CS, Genovese A, Butler MG. Deletion of TOP3B is associated with cognitive
809 impairment and facial dysmorphism. Cytogenet Genome Res. 2016;150(2):106–11.

810 4. Dekker NH, Rybenkov V V, Duguet M, Crisona NJ, Cozzarelli NR, Bensimon D, et al.
811 The mechanism of type IA topoisomerases. Proc Natl Acad Sci. 2002;99(19):12126–
812 31.

813 5. Piñero J, Saüch J, Sanz F, Furlong LI. The DisGeNET cytoscape app: Exploring and
814 visualizing disease genomics data. Comput Struct Biotechnol J. 2021;19:2960–7.

815 6. Wu MN, Littleton JT, Bhat MA, Prokop A, Bellen HJ. ROP, the Drosophila Sec1
816 homolog, interacts with syntaxin and regulates neurotransmitter release in a dosage-
817 dependent manner. EMBO J. 1998;17(1):127–39.

818 7. Schulze KL, Littleton JT, Salzberg A, Halachmi N, Stern M, Lev Z, et al. Rop, a
819 Drosophila homolog of yeast Sec1 and vertebrate n-Sect/Munc-18 proteins, is a
820 negative regulator of neurotransmitter release in vivo. Neuron. 1994;13(5):1099–108.

821 8. Zhang W, Liu HT. MAPK signal pathways in the regulation of cell proliferation in
822 mammalian cells. Cell Res. 2002;12(1):9–18.

823 9. Huang R, Quan Y, Chen J, Wang T, Xu M, Ye M, et al. Osteopontin promotes cell
824 migration and invasion, and inhibits apoptosis and autophagy in colorectal cancer by
825 activating the p38 MAPK signaling pathway. Cell Physiol Biochem. 2017;41(5):1851–
826 64.

827 10. Baker NM, Rajan R, Mondragón A. Structural studies of type I topoisomerases.
828 Nucleic Acids Res. 2009;37(3):693–701.

829 11. Pommier Y, Sun Y, Shar-yin NH, Nitiss JL. Roles of eukaryotic topoisomerases in
830 transcription, replication and genomic stability. Nat Rev Mol cell Biol.
831 2016;17(11):703.

832 12. Nostramo R, Xing S, Zhang B, Herman PK. Insights into the role of P-bodies and stress
833 granules in protein quality control. Genetics. 2019;213(1):251–65.

834 13. Siaw GE-L, Liu I-F, Lin P-Y, Been MD, Hsieh T. DNA and RNA topoisomerase activities
835 of Top3β are promoted by mediator protein Tudor domain-containing protein 3. Proc
836 Natl Acad Sci. 2016;113(38):E5544–51.

837 14. Nakamura A, Amikura R, Hanyu K, Kobayashi S. Me31B silences translation of oocyte-
838 localizing RNAs through the formation of cytoplasmic RNP complex during Drosophila
839 oogenesis. 2001;

840 15. Wilhelm JE, Buszczak M, Sayles S. Efficient protein trafficking requires trailer hitch, a

841 component of a ribonucleoprotein complex localized to the ER in Drosophila. Dev
842 Cell. 2005;9(5):675–85.

843 16. Barbee SA, Estes PS, Cziko A-M, Hillebrand J, Luedeman RA, Coller JM, et al. Staufen-
844 and FMRP-containing neuronal RNPs are structurally and functionally related to
845 somatic P bodies. Neuron. 2006;52(6):997–1009.

846 17. Liu J, Carmell MA, Rivas F V, Marsden CG, Thomson JM, Song J-J, et al. Argonaute2 is
847 the catalytic engine of mammalian RNAi. Science (80-). 2004;305(5689):1437–41.

848 18. Wang M, Ly M, Lugowski A, Laver JD, Lipshitz HD, Smibert CA, et al. ME31B globally
849 represses maternal mRNAs by two distinct mechanisms during the Drosophila
850 maternal-to-zygotic transition. Elife. 2017;6:e27891.

851 19. Lee J, Yoo E, Lee H, Park K, Hur J-H, Lim C. LSM12 and ME31B/DDX6 define distinct
852 modes of posttranscriptional regulation by ATAXIN-2 protein complex in Drosophila
853 circadian pacemaker neurons. Mol Cell. 2017;66(1):129–40.

854 20. Hillebrand J, Barbee SA, Ramaswami M. P-body components, microRNA regulation,
855 and synaptic plasticity. ScientificWorldJournal. 2007;7:178–90.

856 21. Ruscica V, Bawankar P, Peter D, Helms S, Igreja C, Izaurralde E. Direct role for the
857 Drosophila GIGYF protein in 4EHP-mediated mRNA repression. Nucleic Acids Res.
858 2019;47(13):7035–48.

859 22. Lee S, Kolodziej PA. Short Stop provides an essential link between F-actin and
860 microtubules during axon extension. 2002;

861 23. Liu Z, Steward R, Luo L. Drosophila Lis1 is required for neuroblast proliferation,
862 dendritic elaboration and axonal transport. Nat Cell Biol. 2000;2(11):776–83.

863 24. Sidisky JM, Babcock DT. Visualizing synaptic degeneration in adult Drosophila in
864 association with neurodegeneration. JoVE (Journal Vis Exp. 2020;(159):e61363.

865 25. DeJesus-Hernandez M, Mackenzie IR, Boeve BF, Boxer AL, Baker M, Rutherford NJ, et
866 al. Expanded GGGGCC hexanucleotide repeat in noncoding region of C9ORF72 causes
867 chromosome 9p-linked FTD and ALS. Neuron. 2011;72(2):245–56.

868 26. Renton AE, Majounie E, Waite A, Simón-Sánchez J, Rollinson S, Gibbs JR, et al. A
869 hexanucleotide repeat expansion in C9ORF72 is the cause of chromosome 9p21-
870 linked ALS-FTD. Neuron. 2011;72(2):257–68.

871 27. Vatsavayai SC, Nana AL, Yokoyama JS, Seeley WW. C9orf72-FTD/ALS pathogenesis:
872 evidence from human neuropathological studies. Acta Neuropathol. 2019;137:1–26.

873 28. Goodman LD, Prudencio M, Kramer NJ, Martinez-Ramirez LF, Srinivasan AR, Lan M, et
874 al. Toxic expanded GGGGCC repeat transcription is mediated by the PAF1 complex in
875 C9orf72-associated FTD. Nat Neurosci. 2019;22(6):863–74.

876 29. Mignone F, Gissi C, Liuni S, Pesole G. Untranslated regions of mRNAs. Genome Biol.
877 2002;3:1–10.

878 30. Ast G. How did alternative splicing evolve? Nat Rev Genet. 2004;5(10):773–82.

879 31. Black DL. Protein diversity from alternative splicing: a challenge for bioinformatics

880 and post-genome biology. Cell. 2000;103(3):367–70.

881 32. Budagyan B, Loraine A. Gene length and alternative transcription in fruit fly. In:
882 Proceedings 2004 IEEE Computational Systems Bioinformatics Conference, 2004 CSB
883 2004. IEEE; 2004. p. 515–6.

884 33. McGuire AM, Pearson MD, Neafsey DE, Galagan JE. Cross-kingdom patterns of
885 alternative splicing and splice recognition. Genome Biol. 2008;9(3):1–19.

886 34. Fox-Walsh KL, Dou Y, Lam BJ, Hung S, Baldi PF, Hertel KJ. The architecture of pre-
887 mRNAs affects mechanisms of splice-site pairing. Proc Natl Acad Sci.
888 2005;102(45):16176–81.

889 35. Liang J, Wen J, Huang Z, Chen X, Zhang B, Chu L. Small nucleolar RNAs: insight into
890 their function in cancer. Front Oncol. 2019;9:587.

891 36. Han K, Gennarino VA, Lee Y, Pang K, Hashimoto-Torii K, Choufani S, et al. Human-
892 specific regulation of MeCP2 levels in fetal brains by microRNA miR-483-5p. Genes
893 Dev. 2013;27(5):485–90.

894 37. Tushev G, Glock C, Heumüller M, Biever A, Jovanovic M, Schuman EM. Alternative 3'
895 UTRs modify the localization, regulatory potential, stability, and plasticity of mRNAs in
896 neuronal compartments. Neuron. 2018;98(3):495–511.

897 38. Glock C, Biever A, Tushev G, Nassim-Assir B, Kao A, Bartnik I, et al. The translatome of
898 neuronal cell bodies, dendrites, and axons. Proc Natl Acad Sci. 2021;118(43).

899 39. Dewey EB, Parra AS, Johnston CA. Loss of the spectraplakin gene Short stop induces a
900 DNA damage response in Drosophila epithelia. Sci Rep. 2020;10(1):1–13.

901 40. Sanchez-Soriano N, Travis M, Dajas-Bailador F, Gonçalves-Pimentel C, Whitmarsh AJ,
902 Prokop A. Mouse ACF7 and drosophila short stop modulate filopodia formation and
903 microtubule organisation during neuronal growth. J Cell Sci. 2009;122(14):2534–42.

904 41. Prokop A, Beaven R, Qu Y, Sánchez-Soriano N. Using fly genetics to dissect the
905 cytoskeletal machinery of neurons during axonal growth and maintenance. J Cell Sci.
906 2013;126(11):2331–41.

907 42. Valakh V, Walker LJ, Skeath JB, DiAntonio A. Loss of the spectraplakin short stop
908 activates the DLK injury response pathway in Drosophila. J Neurosci.
909 2013;33(45):17863–73.

910 43. Bennett V, Baines AJ. Spectrin and ankyrin-based pathways: metazoan inventions for
911 integrating cells into tissues. Physiol Rev. 2001;81(3):1353–92.

912 44. Thomas GH, Williams JA. Dynamic rearrangement of the spectrin membrane skeleton
913 during the generation of epithelial polarity in Drosophila. J Cell Sci.
914 1999;112(17):2843–52.

915 45. Banks GT, Fisher E. Cytoplasmic dynein could be key to understanding
916 neurodegeneration. Genome Biol. 2008;9(3):1–4.

917 46. Bianco A, Dienstbier M, Salter HK, Gatto G, Bullock SL. Bicaudal-D regulates fragile X
918 mental retardation protein levels, motility, and function during neuronal
919 morphogenesis. Curr Biol. 2010;20(16):1487–92.

920 47. Formicola N, Vijayakumar J, Besse F. Neuronal ribonucleoprotein granules: Dynamic
921 sensors of localized signals. Traffic. 2019;20(9):639–49.

922 48. Greenblatt EJ, Spradling AC. Fragile X mental retardation 1 gene enhances the
923 translation of large autism-related proteins. Science (80-). 2018;361(6403):709–12.

924 49. Lee SK, Xue Y, Shen W, Zhang Y, Joo Y, Ahmad M, et al. Topoisomerase 3β interacts
925 with RNAi machinery to promote heterochromatin formation and transcriptional
926 silencing in Drosophila. Nat Commun. 2018;9(1):4946.

927 51. Gratz SJ, Rubinstein CD, Harrison MM, Wildonger J, O'Connor-Giles KM. CRISPR-Cas9
928 genome editing in Drosophila. Curr Protoc Mol Biol. 2015;111(1):31–2.

929 52. Port F, Bullock SL. Augmenting CRISPR applications in Drosophila with tRNA-flanked
930 sgRNAs. Nat Methods. 2016;13(10):852–4.

931 53. Cunningham F, Allen JE, Allen J, Alvarez-Jarreta J, Amode MR, Armean IM, et al.
932 Ensembl 2022. Nucleic Acids Res. 2022;50(D1):D988–95.

933 54. DeLuca SZ, Spradling AC. Efficient expression of genes in the Drosophila germline
934 using a UAS promoter free of interference by Hsp70 piRNAs. Genetics.
935 2018;209(2):381–7.

936 55. Vazquez-Pianzola P, Adam J, Haldemann D, Hain D, Urlaub H, Suter B. Clathrin heavy
937 chain plays multiple roles in polarizing the Drosophila oocyte downstream of Bic-D.
938 Development. 2014;141(9):1915–26.

939 56. Cox J, Mann M. MaxQuant enables high peptide identification rates, individualized
940 ppb-range mass accuracies and proteome-wide protein quantification. Nat
941 Biotechnol. 2008;26(12):1367–72.

942 57. Consortium U. UniProt: a worldwide hub of protein knowledge. Nucleic Acids Res.
943 2019;47(D1):D506–15.

944 58. Huber W, Von Heydebreck A, Sültmann H, Poustka A, Vingron M. Variance
945 stabilization applied to microarray data calibration and to the quantification of
946 differential expression. Bioinformatics. 2002;18(suppl_1):S96–104.

947 59. Silva JC, Gorenstein M V, Li GZ, Vissers JP. C; Geromanos, SJ Absolute quantification of
948 proteins by LCMSE: A virtue of parallel MS acquisition. Mol Cell Proteomics.
949 2006;5:144–56.

950 60. Silver JD, Ritchie ME, Smyth GK. Microarray background correction: maximum
951 likelihood estimation for the normal–exponential convolution. Biostatistics.
952 2009;10(2):352–63.

953 61. Kammers K, Cole RN, Tiengwe C, Ruczinski I. Detecting significant changes in protein
954 abundance. EuPA open proteomics. 2015;7:11–9.

955 62. Uldry A-C, Maciel-Dominguez A, Jornod M, Buchs N, Braga-Lagache S, Brodard J, et al.
956 Effect of Sample Transportation on the Proteome of Human Circulating Blood
957 Extracellular Vesicles. Int J Mol Sci. 2022;23(9):4515.

958 63. Andrews S. FastQC: a quality control tool for high throughput sequence data.
959 Babraham Bioinformatics, Babraham Institute, Cambridge, United Kingdom; 2010.

960 64. Wang L, Wang S, Li W. RSeQC: quality control of RNA-seq experiments.
961 Bioinformatics. 2012;28(16):2184–5.

962 65. Smith T, Heger A, Sudbery I. UMI-tools: modeling sequencing errors in Unique
963 Molecular Identifiers to improve quantification accuracy. Genome Res.
964 2017;27(3):491–9.

965 66. Martin M. Cutadapt removes adapter sequences from high-throughput sequencing
966 reads. EMBnet J. 2011;17(1):10–2.

967 67. Kim D, Langmead B, Salzberg SL. HISAT: a fast spliced aligner with low memory
968 requirements. Nat Methods. 2015;12(4):357–60.

969 68. Liao Y, Smyth GK, Shi W. featureCounts: an efficient general purpose program for
970 assigning sequence reads to genomic features. Bioinformatics. 2014;30(7):923–30.

971 69. Love MI, Huber W, Anders S. Moderated estimation of fold change and dispersion for
972 RNA-seq data with DESeq2. Genome Biol. 2014;15(12):1–21.

973 70. Core R. TEAM, 2017. R: A language and environment for statistical computing. R
974 Foundation for Statistical Computing, Vienna, Austria. Online https//www r-project
975 org. 2022;

976 71. Castells-Nobau A, Nijhof B, Eidhof I, Wolf L, Scheffer-de Gooyert JM, Monedero I, et
977 al. Two algorithms for high-throughput and multi-parametric quantification of
978 Drosophila neuromuscular junction morphology. J Vis Exp Jove. 2017;(123).

979 72. Szklarczyk D, Franceschini A, Wyder S, Forslund K, Heller D, Huerta-Cepas J, et al.
980 STRING v10: protein–protein interaction networks, integrated over the tree of life.
981 Nucleic Acids Res. 2015;43(D1):D447–52.

982 73. Stoll G, Pietiläinen OPH, Linder B, Suvisaari J, Brosi C, Hennah W, Leppä V, Torniainen
983 M, Ripatti S, Ala-Mello S, Plöttner O, Rehnström K, Tuulio-Henriksson A, Varilo T,
984 Tallila J, Kristiansson K, Isohanni M, Kaprio J, Eriksson JG, Raitakari OT, Lehtimäki T,
985 Jarvelin MR, Salomaa V, Hurles M, Stefansson H, Peltonen L, Sullivan PF, Paunio T,
986 Lönnqvist J, Daly MJ, Fischer U, Freimer NB, Palotie A. Deletion of TOP3β, a
987 component of FMRP-containing mRNPs, contributes to neurodevelopmental
988 disorders. Nat Neurosci. 2013 Sep;16(9):1228-1237. doi: 10.1038/nn.3484. Epub 2013
989 Aug 4. PMID: 23912948; PMCID: PMC3986889.

990 74. Su, S, Xue, Y., Sharov, A., Zhang, Y., Lee, S.K., Martindale, J.L., Li, W., Ku, W.L., Zhao, K.,
991 De, S., Shen, W., Sen, P., Gorospe, M., Xu, D., Wang, W. A dual-activity topoisomerase
992 complex regulates mRNA translation and turnover. Nucleic Acids Res
993 2022;50(12):7013-7033.

994 75. Schiavo G, Greensmith L, Hafezparast M, Fisher EM. Cytoplasmic dynein heavy chain:
995 the servant of many masters. Trends Neurosci. 2013 Nov;36(11):641-51. doi:
996 10.1016/j.tins.2013.08.001.
997 76. Wilkie GS, Davis I. Drosophila wingless and pair-rule transcripts localize apically by
998 dynein-mediated transport of RNA particles. Cell. 2001 Apr 20;105(2):209-19.
999 doi: 10.1016/s0092-8674(01)00312-9. PMID: 11336671.

1000 77. Bullock SL, Ish-Horowicz D. Conserved signals and machinery for RNA transport in
1001 Drosophila oogenesis and embryogenesis. Nature. 2001 Dec 6;414(6864):611-6.
1002 doi: 10.1038/414611a. PMID: 11740552.

1003

Supplementary

Figures S1-S4

Figure S1

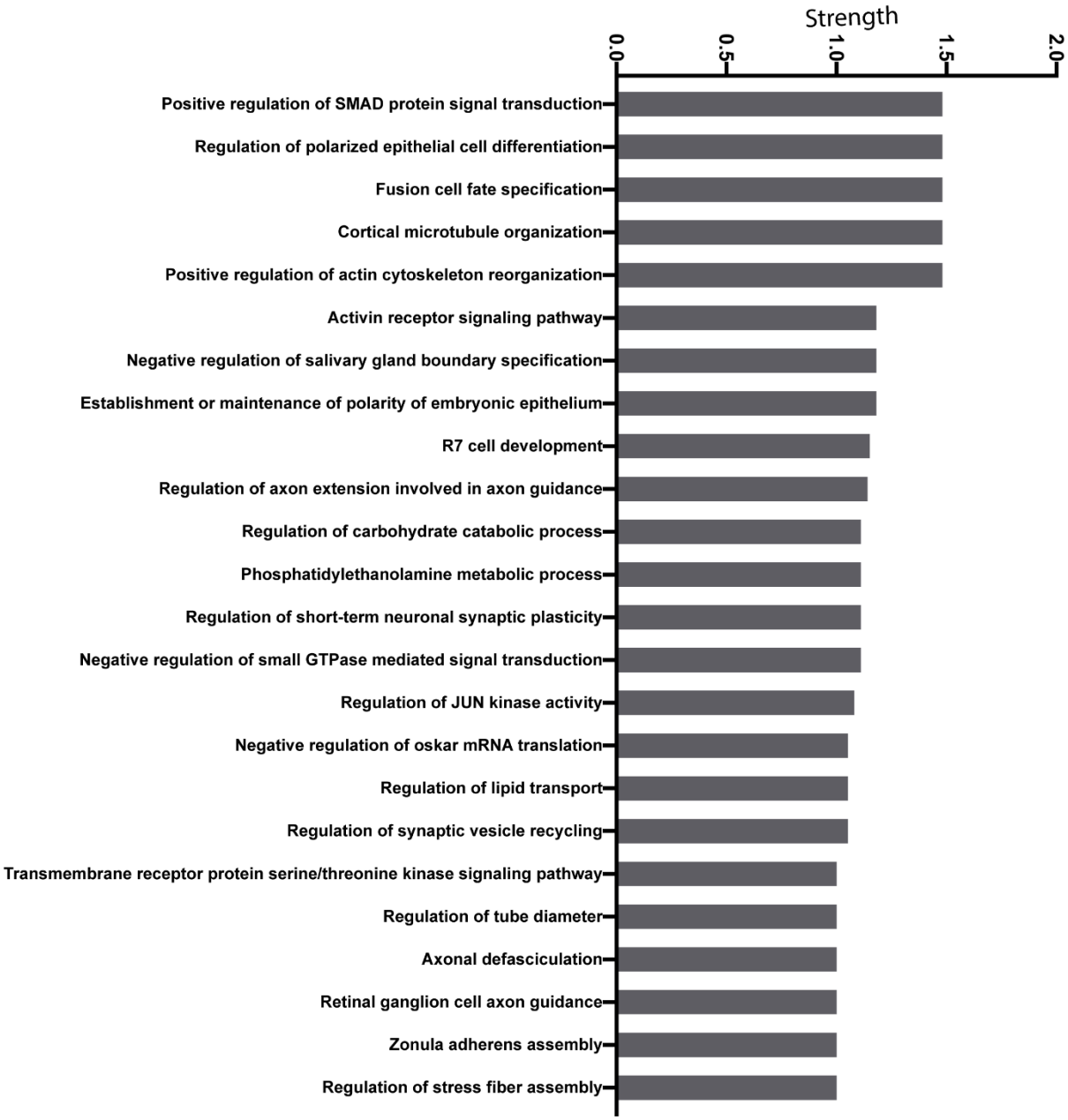

Supplementary Fig. S1: Gene Ontology enrichment for embryonic RNAs that need *Top3β* for their normal expression levels. Strength: Log10 of the enrichment according to StringDB.

Figure S2

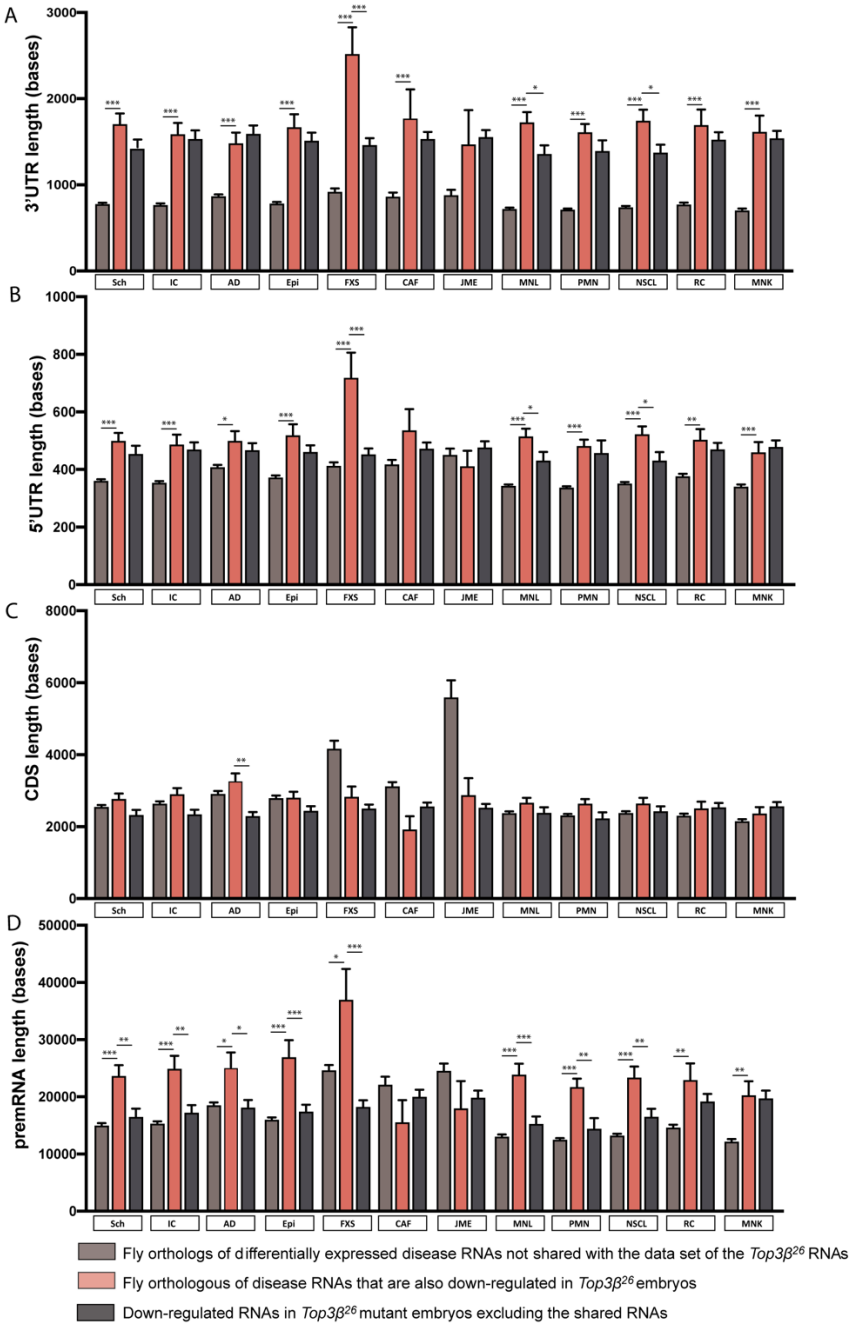

Supplementary Fig. S2: Transcript features for the differentially expressed RNAs from the embryo and the fly homologs of genes associated with the indicated diseases. A, B) mRNAs shared between the two lists show longer UTRs compared to the average fly homolog of the disease mRNA and the average *Top3β* dependent mRNA. **C)** CDS length revealed no significant difference between the three gene lists for each disease (except for AD). **D)** Shared mRNAs show longer pre-mRNAs compared to the average disease-homolg mRNA length and the average length of the embryonic *Top3β*-dependent RNA list. p-value <0.0001=****, p-value <0.001=***, p-value <0.01=**, p-value <0.05=*. Sch: Schizophrenia, IC: Impaired cognition, AD: Autistic Disorders, Epi: Epilepsy, FXS: Fragile X syndrome, CAF: Congenital anomaly of face, JME: Juvenile Myoclonic Epilepsy, MNL: Malignant neoplasm of the lung, PMN: Primary malignant neoplasm, NSCL: Non-Small Cell lung carcinoma, RC: Renal carcinoma, MNK: Malignant neoplasm of the kidney.

Figure S3

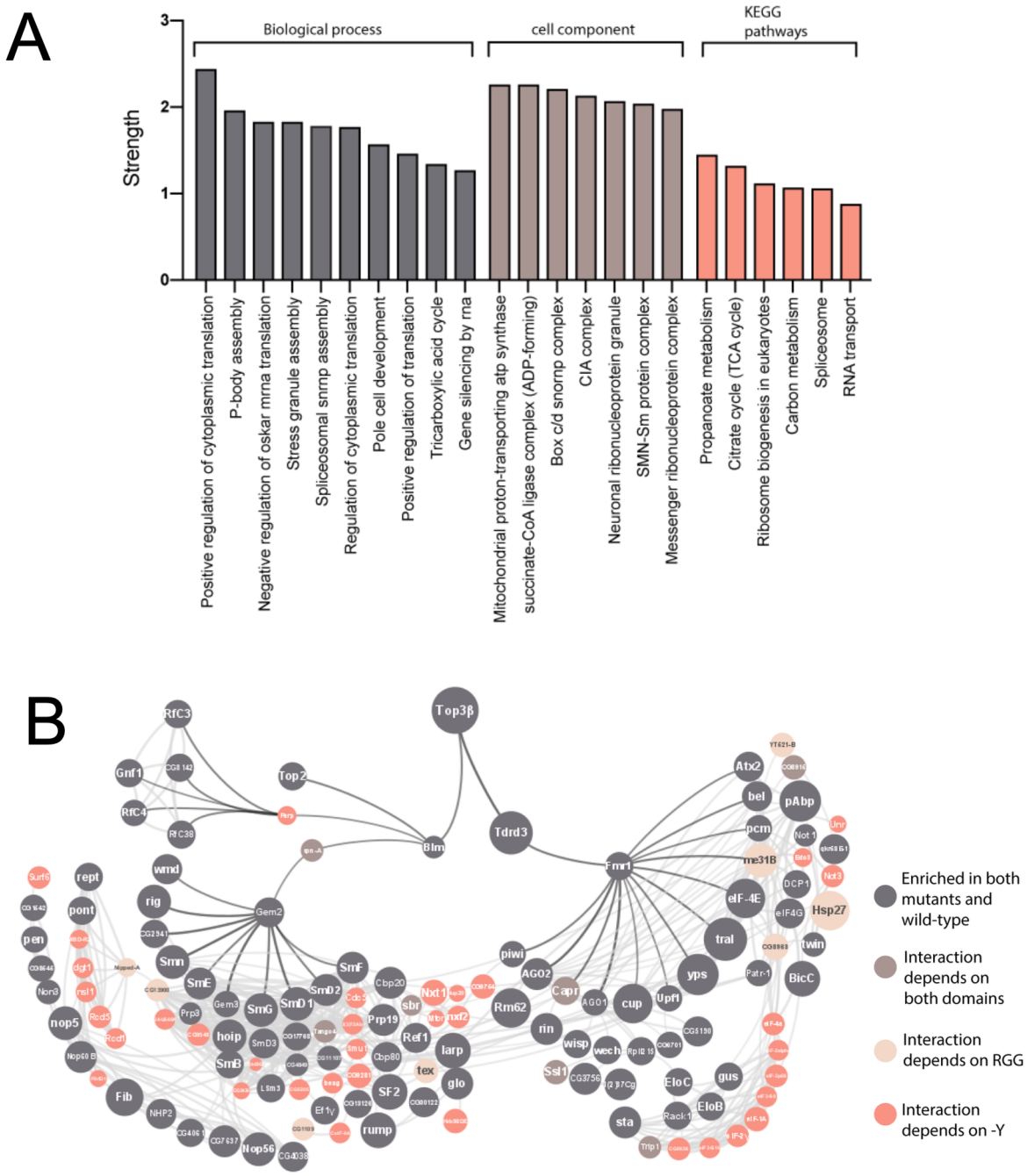

Fig. S3: Pathways and interactions of Drosophila Top3β. A) ***Gene ontology enrichment for Top3β-associated proteins for the top 100 interactors identified in embryonic extracts.*** Immunoprecipitations (IP) on extracts from 0-2 hours old embryos were performed using *Top3β-eGFP* and the *eGFP* control line. Polypeptide components of the IP complexes were analyzed using mass spectrometry (MS) and their abundance was compared to the eGFP control. This resulted in a list of 426 potential complex components with an adjusted p-value <0.01 and log2FC>1 (**Supplementary Table S5).** 89 ribosomal proteins were in this set. A gene ontology enrichment analysis was then performed for the top 100 (according to log2FC) non-ribosomal proteins. This revealed proteins involved in the activation of translation, P-bodies, stress granules, and neural ribonucleoprotein granules, all membrane-less structures involved in storing specific mRNAs during periods of stress or concentrating mRNAs and regulatory proteins (12). Additionally, the interactors were also enriched in several functions related to mitochondria. **B)** ***Proteins enriched in the embryonic protein-IP with their***

physical interactions according to Cytoscape-String. Proteins that ended up further away from Top3β than the ones shown here, were removed from the interaction map. Tdrd3, an established interactor of Top3β (13), was among the top enriched proteins, suggesting that our immunoprecipitation was specific. To assess the role of the Y332 residue and the RGG box in Top3β interactions, IP results were compared with the ones from the *Top3β* mutants *Top3β*^{Y332F}*-eGFP* and *Top3β*$^{\Delta RGG}$*-eGFP*. Among the 337 non-ribosomal binding candidates, 102 needed the Y residue and the RGG box to bind to Top3β-eGFP **(Supplementary Table S5)**. An additional 16 proteins needed the Tyr (but not the RGG) and 23 the RGG box (but not the Y332) for their binding to Top3β. A large fraction of the identified proteins is involved in RNA transport, translation, splicing, mRNA surveillance, and degradation. The physical interaction map of the proteins enriched in the Top3β::GFP IP was created using Cytoscape-String and the results from the mutant analyses were entered into this map. The resulting map resolved into two distinct sub-maps. The left branch connects Top3β functions to its nuclear functions and includes splicing factors. The right branch is enriched in cytoplasmic proteins and includes Tdrd3, FMR1, the piRNA pathway, and translation. The association first Tdrd3 and FMRP has already been described from work with vertebrate cell cultures (74). The interaction of Me31B with Top3β turned out to be dependent on the RGG box. As an RNA helicase, Me31B is a core component of a variety of ribonucleoprotein complexes (RNPs) that participate in translational control and mRNA decapping during embryogenesis, oogenesis, neurogenesis, and neurotransmission (14)(15)(16)(17)(18)(19)(20)(21). Me31B RNPs also containing Tral, eIF4E1, Cup, and pAbp. They are also involved in RNA localization and translational control of maternal mRNAs during oogenesis and embryogenesis (18). These other complex proteins were also enriched in the embryonic Top3β::eGFP IP.

Figure S4

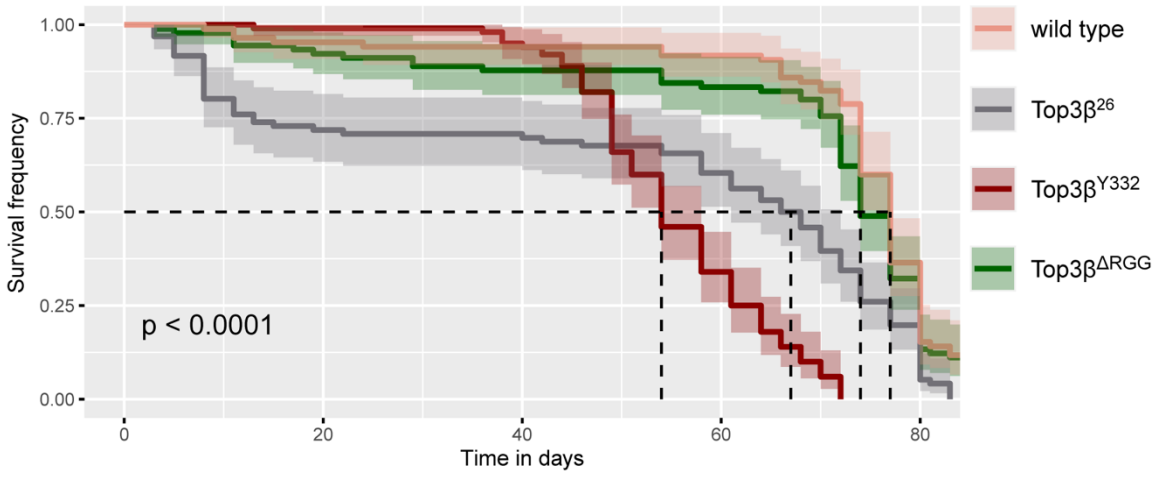

Supplementary Fig. S4: Life span modulation by *Top3β*. The null and the *Y332F* mutants show the strongest effect on survival, but their kinetics differ.

Legends for

Supplementary

Tables S1-S6

Supplementary Tables S1-S6

Supplementary Table S1) embryo transcriptomics lists the filtered Top3β transcriptomics results (with adjusted p-value <0.05 and absolute log2 fold change >1) from embryos. Columns C, D: Top3β^{26} vs wild-type embryos. Columns E, F: Top3β$^{\Delta RGG}$ vs wild-type embryos. Columns G, H: Top3β^{Y332F} vs wild-type embryos. Columns I: gene name (symbol), Columns J-M: length of indicated RNA features. The embryo background list (2nd sheet) shows the length of the RNA features for all transcripts identified.

Supplementary Table S2) List of Drosophila melanogaster homologs of differentially expressed genes associated with those neurological diseases and cancers with which human *Top3β* had been associated**.**

Supplementary Table S3) List of RNAs (and gene names) that were purified with Top3β::GFP from embryonic extract. Enrichment of an RNA in the wild-type IP versus the null mutant was used to select the best target RNAs. RNA features are indicated for these RNAs, too.

Supplementary Table S4) List of the top targets of Top3β::GFP with their RNA features indicated.

Supplementary Table S5) List of proteins co-immunoprecipitated (co-IP) with Top3β::GFP. Enrichment in comparison to GFP-only IPs and co-IPs with mutant versions of Top3β*::GFP are shown. The dependence of the interaction with the RGG domain and the Y332 residue are shown.

Supplementary Table S6) Oligos, primers and fly lines used in this study.